Received: 11 January 2026 | Revised: 31 March 2026 | Accepted: 3 May 2026

DOI: 10.1002/ame2.70230

ORIGINAL ARTICLE

Chrysina lleviatesp ressure overload–induced myocardial remodelingt hroughr egulating the PI3K/AKT/NRF2 pathway–mediated oxidative stress response

Yijia Wang[1] | **Xing Feng**[1] | **Shuhui Zhao**[1] | **Yuchong Fu**[1] | **Ao Zhang**[1] | **Xiaofeng Shen**[2] | **Bowen Yu**[2] | **Yihao Wang**[2] | **Jiahui Lin**[2] | **Bing Zhang**[3] | **Weiping Ji**[2,4] | **Lianpin Wu**[5,6] | **Xiaoling Guo**[1,5,6]

[1]Basic Medical Research Center, The Second Affiliated Hospital and Yuying Children's Hospital of Wenzhou Medical University, Wenzhou, China

[2]Department of General Surgery, The Second Affiliated Hospital and Yuying Children's Hospital of Wenzhou Medical University, Wenzhou, China

[3]Engineering Research Center of Techniques and Instruments for Diagnosis and Treatment of Congenital Heart Disease, Institute of Developmental and Regenerative Medicine, Xin Hua Hospital, School of Medicine, Shanghai Jiao Tong University, Shanghai, China

[4]National Cancer Center/National Clinical Research Center for Cancer/Cancer Hospital, Chinese Academy of Medical Sciences and Peking Union Medical College, Beijing, China

[5]Zhejiang-Ireland Joint Laboratory for Precision Diagnosis and Treatment of Valvular Heart Diseases, The Second Affiliated Hospital of Wenzhou Medical University, Wenzhou, China

[6]Department of Cardiology, The Second Affiliated Hospital of Wenzhou Medical University, Wenzhou, China

Correspondence
Weiping Ji, Department of General Surgery, the Second Affiliated Hospital and Yuying Children's Hospital of Wenzhou Medical University, Wenzhou, Zhejiang, China.
Email: jiweiping19841022@126.com

Lianpin Wu, Zhejiang-Ireland Joint Laboratory for Precision Diagnosis and Treatment of Valvular Heart Diseases, the Second Affiliated Hospital of Wenzhou Medical University, Wenzhou, Zhejiang, China.
Email: 198019@wzhealth.com

Xiaoling Guo, Basic Medical Research Center, The Second Affiliated Hospital and Yuying Children's Hospital of Wenzhou Medical University, 109 Xueyuan West Road, Wenzhou 325027, Zhejiang, China.
Email: guoxling@wmu.edu.cn

Fundingi nformation
The Key Research and Development Program of Zhejiang Province, Grant/Award Number: 2023C03018; Natural

Abstract

Background: Oxidative stress plays a pivotal role in the pathogenesis of heart failure and is closely linked to myocardial remodeling, which includes myocardial hypertrophy and fibrosis. Chrysin (CHR) has multiple medicinal effects such as antioxidant, anti-inflammatory, and anti-apoptosis. This research seeks to investigate whether CHR can protect against pressure overload–induced myocardial remodeling and to explore the underlying mechanism.

Methods: Transverse aortic constriction (TAC) surgery was conducted to establish a model of cardiac hypertrophy on male C57BL/6J mice. A model of cardiomyocyte hypertrophy in H9C2 cells induced by angiotensin II (Ang II) was also established.

Results: The results showed that CHR significantly improved survival and cardiac function, reduced myocardial hypertrophy and fibrosis, inhibited the expression of inflammatory mediators TNF-α and IL-1β, suppressed cell apoptosis rate, downregulated the levels of Bcl-2 Associated X protein (BAX) and Cleaved-Caspase-3, and upregulated B-cell lymphoma/leukemia 2 (BCL-2) expression in TAC surgical mice or Ang II-treated H9C2 cells. CHR could also upregulate the levels of antioxidant enzymes SOD1 and HO-1 by mediating the nuclear translocation and expression of NRF2 to

Yijia Wang, Xing Feng, and Shuhui Zhao have contributed equally to this work.

Science Foundation of Zhejiang Province, Grant/Award Number: LY24H020008; Jie Bang Gua Shuai Project of Wenzhou Science and Technology Bureau, Grant/Award Number: ZY2023022 and ZY2024019

counteract oxidative stress response. The further mechanism investigation utilizing bioinformatics analysis and western blot revealed that the disease of heart failure is associated with the phosphatidylinositol-3-kinase (PI3K)/serine/threonine-protein kinase B (AKT) signaling pathway.

Conclusions: Collectively, our findings demonstrated that CHR might exert the improvement effects on pressure overload–induced myocardial remodeling with hypertrophy and fibrosis through regulating the PI3K/AKT/NRF2 pathway–mediated oxidative stress response to alleviate myocardial cell inflammation and apoptosis, suggesting that CHR may be a promising therapeutic agent for cardiac diseases induced by pressure overload.

KEYWORDS
apoptosis, chrysin, inflammation, myocardial remodeling, oxidative stress

1 | INTRODUCTION

The main feature of heart failure is impaired left ventricular systolic function, accompanied by several pathological changes such as myocardial hypertrophy, fibrosis, apoptosis, and inflammation.[1] Heart failure is regarded as the terminal stage of multiple heart diseases, including myocardial infarction, hypertension, and myocarditis.[2,3] The mortality rate of heart failure is significantly high, which imposes a big burden on both the medical system and on the families of patients.[4,5] Myocardial remodeling constitutes a key pathological driver underlying the progression of heart failure.[6] Myocardial remodeling, characterized by hypertrophy, indicates an adaptive compensatory response of the heart to preserve contractile function. However, under persistent pressure overload, this compensatory mechanism progressively transitions into decompensation, ultimately leading to heart failure.[7] Myocardial remodeling is mainly manifested as myocardial hypertrophy, extracellular matrix deposition, and fibrosis.[8] The excessive pressure load on the left ventricle, resulting from aortic valve stenosis or hypertension, can potentially lead to heart failure in clinical situations.[9] Consequently, it is imperative to understand the pathophysiological mechanism of myocardial remodeling and to explore innovative therapeutic strategies aimed at effectively mitigating the progression of myocardial remodeling.

Oxidative stress response is closely correlated with the pathogenic mechanism of myocardial remodeling.[10] Accumulating evidences from both experimental and clinical studies indicate that oxidative stress is significantly aggravated in myocardial remodeling and heart failure.[10] Nuclear factor erythroid 2-related factor 2 (NRF2) is a key downstream effector of the phosphatidylinositol-3-kinase (PI3K)/serine/threonine-protein kinase B (AKT) pathway; at the same time, it functions as a primary regulatory factor in antioxidant response.[11] NRF2 activation exerts a cytoprotective effect against oxidative stress by upregulating the expression of antioxidant enzymes heme oxygenase-1 (HO-1) and superoxide dismutase (SOD).[12]

Chrysin (CHR) is a bioactive flavone extracted from the blue passion flower, propolis, honey, and others.[13] This substance exerts many different pharmacological properties, such as antioxidant, anti-inflammatory, antibacterial, antiapoptotic, antidiabetic, hepatoprotective, and nephroprotective activities.[14,15] Research work has shown that CHR administration decreased malondialdehyde levels and simultaneously enhanced the function of primary reactive oxygen species (ROS)–scavenging enzymes, including SOD, catalase, and glutathione *S*-transferase.[16] CHR could regulate the PI3K/AKT pathway in neuroblast cells under oxygen–glucose deprivation condition.[17] Additionally, CHR has been shown to mitigate myocardial oxidative damage triggered by a high-fat diet through upregulating NRF2.[18] Prior study has also demonstrated that matairesinol could alleviate pressure overload–induced cardiac remodeling through regulating the PI3K/AKT/FOXO1 pathway.[19]

To date, the effects of CHR on pressure overload–induced myocardial remodeling have not been investigated. Due to its excellent efficacy and low toxicity, CHR may be regarded as an available antioxidant for cardiovascular diseases. We will explore whether CHR alleviates myocardial remodeling with cardiac hypertrophy and fibrosis in transverse aortic constriction (TAC) surgical mice and angiotensin II (Ang II)–treated H9C2 cells as well as try to elucidate the potential mechanism.

2 | MATERIALS AND METHODS

2.1 | Reagentp rocessing

CHR powder (Aladdin, Shanghai, China) was dissolved in a solution consisting of 50% PEG300 (MedChemExpress, Shanghai, China) and 50% NaCl (Aladdin). All reagents at working concentration were freshly prepared and used immediately. For in vivo experiment, 150 mg/kg of CHR solution was prepared 2 h earlier based on our pre-experimental concentration exploration and previous report.[20] The optimal working concentrations of CHR and Ang II

(MedChemExpress) applied in in vitro experiments were determined based on cell counting kit-8 (CCK-8) assays.

2.2 | Animals

Six-week-old male C57BL/6J mice were obtained from Weitong Lihua Laboratory Animal Technology (Jiaxing, China). They were housed in a specific-pathogen-free animal facility under a 12-hour light–dark cycle. The ambient temperature was controlled at 23 ± 2°C, and ambient humidity was between 45% and 55%. All mice were provided free access to food and water. After a 1-week acclimatization period to laboratory conditions, the corresponding experiments were performed.

2.3 | Mouse TACm odel

TAC surgery was conducted according to previous studies.[21] Briefly, C57BL/6J mice were subjected to anesthesia using 3% isoflurane and then immobilized on the operating table. They were then connected to a small animal ventilator through tracheal intubation to prevent pneumothorax during operation. An incision ~5 mm in length was made along the sternum body, and the thymus was retracted to expose the aortic arch. A 7–0 nylon suture was passed through the connective tissue between the brachiocephalic trunk and the left common carotid artery. Then, a 27G needle was carefully positioned as a spacer for ligation. Subsequently, after gentle removal of the needle, the surgical area was prepared for thoracic suturing, and the wound was disinfected with iodophor. Once the mice resumed spontaneous respiration, they were disconnected from the ventilator. Mice were assigned randomly to four experimental groups ($n = 10$ per group): sham group, CHR group, TAC group, and TAC + CHR group. Mice in the sham group or the CHR group underwent the same surgical procedure, but TAC surgery was not performed. After TAC surgery, mice in the CHR and the TAC + CHR groups were orally administered 150 mg/kg of CHR for 28 consecutive days. Mice in the sham group as well as the TAC group daily received an equal volume of 0.9% saline by oral gavage.

2.4 | Echocardiography

Cardiac function parameters of mice across all experimental groups were assessed 28 days after TAC surgical operation. Mice were anesthetized with isoflurane; their chest hair was removed, and then they were positioned supine on a conductive sheet with their limbs secured. The chest region was covered with an ultrasound coupling agent prior to detection. Once the heart rate stabilized between 400 and 450 beats per min, ultrasound images of the left ventricular long axis were obtained using a 30-MHz mouse ultrasound probe (VisualSonics Vevo 2100, Canada), which was positioned at 30° to the long axis of the mouse's body. Subsequently, the probe was rotated clockwise by 90° to obtain the short-axis ultrasound images. Utilizing the clearly visible cross section of the papillary muscle, two hyperechoic clusters were identified as a reference, and three complete cardiac cycles were recorded using M-mode ultrasound. Data were then conducted to determine parameters such as the left ventricular fractional shortening (LVFS) and the left ventricular ejection fraction (LVEF).

2.5 | Histopathological staining

Each mouse heart was subjected to perfusion using 0.9% physiological saline, subsequently excised, washed with phosphate-buffered saline (PBS), and fixed in 4% paraformaldehyde at room temperature for 24 h.[22,23] After fixation, the tissues were dehydrated through a graded ethanol series (70%, 80%, 90%, 95%, and 100%), cleared in xylene, and embedded in paraffin. Transverse sections (5 μm thick) were obtained using a paraffin microtome (Leica, Hesse-Darmstadt, Germany). The paraffin sections were placed in an oven and heated for 2 h. After the tissues were dewaxed with xylene and dehydrated through a graded ethanol series, they were stained with hematoxylin and eosin, Masson's trichrome, and Tianwolf scarlet. Finally, the tissue sections were mounted using neutral balsam and allowed to dry completely. Their morphological characteristics and the degree of fibrosis were examined using a case scanner (KFBIO, KFPRO-005, Ningbo, China). ImageJ software (version 1.54) (NIH, MD, USA) was used to perform quantitative assessment.

2.6 | Immunohistochemistry

Paraffin-embedded sections of mouse cardiac tissues were prepared based on the aforementioned procedure. After the tissues were dewaxed and dehydrated through a graded ethanol and xylene series, we performed antigen retrieval using sodium citrate buffer. Once the samples had cooled naturally, they were rinsed with PBS. Endogenous peroxidase activity was then blocked. The tissue sections were then placed in 5% bovine serum albumin (BSA) at room temperature for 1 h. The samples were incubated overnight with primary antibodies (presented in Table S1) at 4°C. Then these samples were rinsed with PBS. The sections were treated with enzyme-conjugated secondary antibodies (1:50, Beyotime, Shanghai, China) at 37°C for 2 h. 3,3'-Diaminobenzidine (DAB) chromogenic solution was used to treat the samples, which were monitored under a light microscope until the background turned light brown. After the samples were washed with PBS, they were counterstained with hematoxylin for several minutes. Then, the samples were washed again with running water. The stain was cleared using a gradient of ethanol and xylene. The prepared slides were mounted with neutral resin. After the slides became dry, the extent of fibrosis and inflammatory infiltration in each tissue sample was assessed utilizing a case scanner. Subsequent quantitative assessment was performed using ImageJ software (version 1.54).

2.7 | Wheat germ agglutinin staining

The prepared paraffin sections were dewaxed and dehydrated through a graded ethanol and xylene series, and then immersed in sodium citrate solution to facilitate antigen retrieval. After the sections were cooled naturally and washed thrice with PBS, wheat germ agglutinin (WGA) staining solution (Thermo Fisher, MA, USA) was employed to treat the sections for 1 h at room temperature. Subsequently, these samples were mounted with 4',6-diamidino-2-phenylindole (DAPI)-containing antifade medium. The cellular morphology was observed using a Keyence fluorescence scanning microscope (BZ-X100, Keyence Corporation, Osaka, Japan), and ImageJ software (version 1.54) was employed to conduct quantitative analysis.

2.8 | TUNELs taining

Mouse cardiac tissue paraffin-embedded sections were prepared and treated using the aforementioned method. To prepare the cell climbing samples, the coverslips with cells were initially fixed at ambient temperature using 4% paraformaldehyde for 30 min. After having washed with PBS, these cell coverslips were treated with 0.3% PBS-Triton X-100 for 10 min for permeabilization. According to the manufacturer's instructions, both tissue sections and cell climbing samples were treated with proteinase K at 37°C for 30 min. After having washed with PBS, we incubated the samples with the prepared terminal deoxynucleotidyl transferase-mediated dUTP nick end labeling (TUNEL) working solution (E-Ck-A320, Elascience, China) at 37°C for 1 h and then washed with PBS. The converter-peroxidase (POD) reagent and DAB chromogenic substrate were subsequently used in sequence to treat samples. Finally, the samples were counterstained with DAPI. The apoptotic cells were observed using a Keyence fluorescence scanning microscope. The apoptotic cells were quantitatively counted using ImageJ software (version 1.54).

2.9 | H9C2 cell culture and treatment

We cultured H9C2 cells in high-glucose Dulbecco's modified Eagle's medium (Thermo Fisher) containing 10% fetal bovine serum (Gibco, USA) and 1% penicillin/streptomycin. Then they were incubated at 37°C with 5% CO_2. To determine the optimal working concentration of Ang II, H9C2 cells were exposed to varying concentrations of Ang II. Subsequently, based on the working concentration of the Ang II–induced cardiomyocyte hypertrophy model, H9C2 cells were treated with different doses of CHR to determine its best concentration using the CCK-8 assay. The experimental groups were as follows: control group, CHR group, Ang II group, Ang II + CHR group, and Ang II + CHR + 740Y-P (PI3K agonist) group. The Ang II + CHR or the Ang II + CHR + 740Y-P group was treated with Ang II 24 h earlier and then treated with either CHR or a combination of CHR and 740Y-P for another 24 h. The concentration of 740Y-P was set at 20 μmol/L according to previous studies.[24]

2.10 | CCK-8a ssay

The CCK-8 kit (NCM, Suzhou, China) was used to analyze the viability of H9C2 cells with different treatments. H9C2 cells were seeded into 96-well plates at a density of 5×10^3 cells per well and cultured for 24 h in a 5% CO_2 incubator at 37°C. Subsequently, H9C2 cells were incubated with different concentrations of Ang II (0, 0.01, 0.1, 1, 10, 100, and 1000 nmol/L) or CHR (0, 50, 100, 150, 200, and 250 nmol/L), and maintained in the incubator for another 24 h. For the Ang II + CHR group, H9C2 cells were first subjected to Ang II for 24 h; then the medium was replaced with a fresh medium containing different concentrations of CHR (50, 100, 150, and 200 nmol/L) for an additional 24 h. Finally, a mixture of 90 μL of fresh medium and 10 μL of CCK-8 solution was added to each well and incubated at 37°C for 1 h. A microplate reader (version 7.1, Thermo Fisher) was used to detect the absorbance at 450 nm.

2.11 | Annexin V and PI assay

The annexin V-allophycocyanin/propidium Iodide (V-APC/PI) apoptosis assay kit (Becton Dickinson, NJ, USA) was used to detect apoptosis. Initially, the culture supernatant of cells was aspirated; then the cells were digested using trypsin free of ethylenediaminetetraacetic acid (EDTA) (Gibco). A total of ~1×10^5 cells were washed with precooled PBS and centrifuged. Then, we used 100 μL of 1× annexin V binding buffer to resuspend the cells and added 5 μL of annexin V-APC and 5 μL of PI. The mixture was incubated for 20 min under light-free conditions. Finally, 400 μL of 1× annexin V binding buffer was added to the mixture, and the samples were analyzed using flow cytometry (Beckman, CA, USA).

2.12 | ROSd etection

ROS production in H9C2 cells in each group was detected using flow cytometry. After the different treatments, the culture supernatant of H9C2 cells was removed, and diluted 2',7'-dichlorodihydr ofluorescein diacetate (DCFH-DA) (10 μmol/L, Solarbio) was added to each well. Then, H9C2 cells were incubated for 20 min at 37°C. Then, they were digested by trypsin free of EDTA and centrifuged. Subsequently, they were suspended in precooled PBS as the washing buffer. Finally, the intracellular ROS levels were assessed using flow cytometer (Beckman).

2.13 | Immunofluorescences taining

We subjected cells in all groups to 4% paraformaldehyde for 30 min. Then, we washed the cells with PBS and permeabilized them using 0.5% PBS-Triton X-100 for 5 min. We blocked the samples with 5% BSA over a 1-hour period. Thereafter, the cells were treated with a primary antibody (provided in Table S1) at 4°C for 14 h. Next, we

washed the cells with PBS and then incubated with fluorochrome-conjugated secondary antibodies for 2 h at room temperature. Subsequently, they were mounted using a DAPI-containing antifade mounting medium and stored in the dark. Finally, a Keyence fluorescence microscope was used to obtain images.

2.14 | Differentially expressed genes and pathway enrichment analysis

RNA-seq data were downloaded from the comprehensive gene expression database (GEO) with accession number GSE175764, which includes heart tissue samples from healthy individuals ($n = 5$) and heart failure individuals with myocardial remodeling ($n = 5$). The experimental data were analyzed using R software (version 4.5.0). To identify potential pathogenic factors, we employed the DESeqDataSetFromMatrix function in the DESeq2 package (version 1.48.1) for data format conversion and then identified differentially expressed genes (DEG) between two groups using the DESeq2 package. The significant DEGs met an absolute log2 fold change (FC) of ≥ 1 and a corrected *p*-value (false discovery rate) of < 0.05. The volcano plot of DEGs was constructed using the ggplot2 package in R software, whereas the gene heat map of DEGs was prepared using the pheatmap package (version 1.0.13). The clusterProfiler package (version 4.16.0) facilitated gene ontology (GO) pathway and function enrichment analysis to elucidate the biological roles and underlying pathways associated with the DEGs. In addition, we established a threshold of < 0.05 for the corrected *p*-values to perform pathway enrichment analysis and explore the interconnections among them.

2.15 | Westernb lot

Approximately 50 mg of left ventricular tissues was collected from the hearts of mice in each group. RIPA lysate (Solarbio, Beijing, China) was supplemented with protease and phosphatase (Solarbio) inhibitors (100:1), and the tissues were homogenized using a tissue homogenizer (60 Hz, 90 s). The homogenate was allowed to stand at 4°C for 30 min and then centrifuged (12 000 *g*, 30 min, 4°C). The supernatant was collected for protein extraction. In the cell experiment, H9C2 cells from each group were washed with PBS, and RIPA lysis buffer containing phosphatase and protease inhibitors was added. The cells were lysed on ice for 30 min, and the cell lysates were scraped and collected. After centrifugation using the aforementioned condition, the supernatant was obtained.

Protein concentration was determined using the Bicinchoninic acid (BCA) protein quantification kit (NCM). An equal amount of protein (40 μg per lane) was loaded for each sample, which was separated using 7.5%, 10%, or 12.5% sodium dodecyl sulfate–polyacrylamide gel. Then, the proteins were transferred onto polyvinylidene fluoride membranes (Thermo Fisher), which were blocked with 5% skimmed milk for 2 h. Subsequently, these membranes were treated with primary antibodies (Table S1) at optimized dilution at 4°C overnight and then washed with Tris-buffered saline with Tween 20. The membranes were then incubated with horseradish peroxidase–conjugated rabbit or mouse secondary antibodies at a dilution of 1:1000 for 2 h at room temperature and rinsed with TBST. Finally, the protein bands were detected using the enhanced chemiluminescence chromogenic kit (EpiZyme, Shanghai, China) under the ChemiDoc XRS imaging system (Bio-Rad, CA, USA). To ensure signal linearity, membranes were exposed for different durations, and nonsaturated images were used for densitometric analysis. Glyceraldehyde 3-phosphate dehydrogenase (GAPDH) was used as the internal reference. The target protein expression levels were normalized to GAPDH and expressed as FC relative to the control group.

2.16 | Real-time quantitative polymerase chain reaction

Trizol reagent was employed to isolate total RNA from mouse cardiac tissues and H9C2 cells (Invitrogen, CA, USA). The quantification concentration of RNA was analyzed utilizing a NanoDrop spectrophotometer (Thermo Fisher). Complementary DNA was synthesized by reverse transcription using the HiScript II Q RT SuperMix reverse transcription kit (Vazyme, Nanjing, China). Real-time quantitative polymerase chain reaction (RT-qPCR) was executed using the Bio-Rad CFX Manager system, with *Gapdh* serving as the internal reference gene. The quantitative analysis of each gene was performed using the $2^{-\Delta\Delta Ct}$ method. The details of all primers are presented in Table S2.

2.17 | Statisticala nalysis

Data are expressed as mean ± standard deviation and were processed using GraphPad Prism, version 9 (CA, USA). In all figure legends, *n* denotes the number of biological replicates. We used Student's *t*-test to compare two groups and one-way analysis of variance (ANOVA) to compare each group, with Dunnett's multiple comparison method applied subsequently. A *p*-value < 0.05 was considered significant, whereas a *p*-value > 0.05 was considered not significant (ns).

3 | RESULTS

3.1 | CHR improved cardiac function and myocardial hypertrophy of mice subjected to TAC surgery

To explore the optimal in vivo dose of CHR, combined with the reported effective dose of CHR (50 mg/kg) in other studies,[25,26] another dose of CHR (150 mg/kg) was investigated in this study. LVEF and LVFS, two critical indicators for cardiac function assessment, were measured using echocardiography.[27] Our results demonstrated that in TAC surgical mice, the 150-mg/kg CHR treatment exhibited

significant improvement in cardiac function than the 50-mg/kg CHR treatment, specifically LVEF and LVFS (Figure S1A,B). Furthermore, Western blot analysis also revealed that in TAC surgical mice, the expression of hypertrophic markers myosin heavy chain 7 (MYH7) and atrial natriuretic peptide (ANP), along with myocardial fibrosis–related proteins collagen I and collagen III, was significantly downregulated by the 150-mg/kg CHR treatment compared to the 50-mg/kg CHR treatment (Figure S1C,D). Therefore, based on its superior therapeutic effects in improving cardiac function as well as reducing hypertrophic and fibrotic markers compared to the 50-mg/kg dose, the working dose of CHR was set at 150 mg/kg for subsequent experiments.

The probability of survival in each group was assessed, revealing that mice in both the sham-operated and the CHR groups exhibited complete survival, whereas the survival rates of mice in the TAC and the TAC+CHR groups were 73.3% and 86.7% respectively, indicating that CHR could improve the survival rate of mice subjected to TAC surgery (Figure 1A). Additionally, we used echocardiography to evaluate the cardiac function of mice in all groups (Figure 1B). Echocardiography results showed that compared to the sham group, there was a significant decline in LVEF and LVFS levels in the TAC group, and there was no significant difference in the relevant parameters between the sham and the CHR groups. However, the TAC+CHR group exhibited significant improvement in LVEF and LVFS levels in contrast to the TAC group (Figure 1C). Besides, the heart weight-to-body weight (HW/BW) ratio and the left ventricular weight-to-body weight (LW/BW) ratio of mice were statistically elevated in the TAC group, relative to the sham group or the CHR group, but CHR intervention could effectively reverse this trend (Figure 1D). We further validated the expression levels of myocardial hypertrophy–associated indexes such as MYH7, brain natriuretic peptide (BNP), and ANP, using RT-qPCR (Figure 1E) and Western blot (Figure 1F) assays. The findings indicated that the messenger RNA (mRNA) and the protein expression of MYH7, BNP and ANP was significantly elevated in the TAC group relative to the sham and the CHR groups, which could be significantly restrained by CHR treatment (Figure 1E,G). To visually assess the effects of CHR on myocardial hypertrophy, the standardized images of mouse hearts were obtained from each group, showing that compared with the sham or the CHR group, the heart size of the TAC group was substantially larger, but CHR administration could alleviate it in the TAC group significantly (Figure 1H). Further evidences from HE staining and WGA staining showed that the cross-sectional area of cardiomyocytes, along with the thickness of the left ventricular septum and posterior wall, increased, and the intercellular space reduced in the TAC group relative to the sham or the CHR group, but CHR intervention significantly abrogated these phenotypes (Figure 1H,I). Collectively, these outcomes suggested that CHR could ameliorate the cardiac dysfunction and myocardial hypertrophy of mice subjected to TAC surgery.

3.2 | CHRa lleviated myocardialf ibrosis of TAC surgical mice

To determine the role of CHR in heart failure–associated myocardial fibrosis in TAC surgical mice, we performed Masson's trichrome staining (Figure 2A). Our findings revealed that relative to the sham and the CHR groups, substantial collagen deposition, namely fibrosis in the interstitial spaces and surrounding blood vessels, was prominently observed in the TAC group, and CHR treatment significantly lowered collagen distribution in these areas of TAC surgical mice, with a more uniform distribution pattern (Figure 2B). Additionally, we quantitatively analyzed the proportion of collagen types using polarized light microscopy (Figure 2C). The results showed that compared with the TAC group, the collagen III level in the TAC+CHR group significantly increased (Figure 2D). Immunohistochemical analysis (Figure 2E) further demonstrated that the number of Transforming growth factor-beta (TGF-β) positive cells in the TAC group was higher than that in the sham or the CHR group, but CHR intervention could significantly decrease the number of TGF-β positive cells in mice subjected to TAC surgery (Figure 2F). Additionally, the expression abundances of TGF-β and collagen I associated with myocardial fibrosis were assessed using Western blot (Figure 2G) and RT-qPCR (Figure 2I). Quantitative analysis results indicated that compared to the sham or the CHR group, the levels of TGF-β and collagen I were statistically upregulated in the TAC group, but there was a conspicuous decrease in TGF-β and collagen I in the TAC+CHR group (Figure 2H,I). These findings suggested that CHR could effectively mitigate myocardial fibrosis of mice subjected to TAC surgery.

3.3 | CHRa ttenuatedc ardiomyocyteo xidative stress, inflammation, and apoptosis of TAC surgical mice

Pressure overload–induced heart failure is inevitably accompanied by oxidative stress and inflammatory reaction in cardiomyocytes.[19]

FIGURE 1 Chrysin (CHR) improved the cardiac function and myocardial hypertrophy of mice subjected to transverse aortic constriction (TAC) surgery. (A) The survival rates of mice in each group. (B) The cardiac function of mice in different groups using echocardiography. (C) The quantitative statistics of left ventricular ejection fraction (LVEF) and left ventricular fractional shortening (LVFS). (D) The statistical analysis of the heart weight/body weight ratio (HW/BW) and the left ventricular weight/body weight ratio (LW/BW). (E) The messenger RNA (mRNA) expression levels of Myh7, Nppb, and Nppa. (F) The protein expression of MYH7, ANP, and BNP using Western blot. (G) The quantitative statistics of protein bands. (H) Gross comparison of hearts in each group (left), hematoxylin and eosin (HE) staining (middle). Scale bar = 2.5 mm. Imaging area: Transverse section of the whole heart. Fluorescence staining of wheat germ agglutinin, right (WGA). Scale bar = 50 μm. Imaging area: Mid-left ventricular transverse section with papillary muscles. (I) The quantitative statistics of the cross-sectional area of cardiomyocytes in each group. All images were obtained from transverse sections (5 μm thick). All data are presented as mean ± SD (standard deviation). $n = 5–6$; $^{*}p < 0.05$, $^{**}p < 0.01$, and $^{***}p < 0.001$ indicate significant differences; and ns > 0.05 means no significant difference.

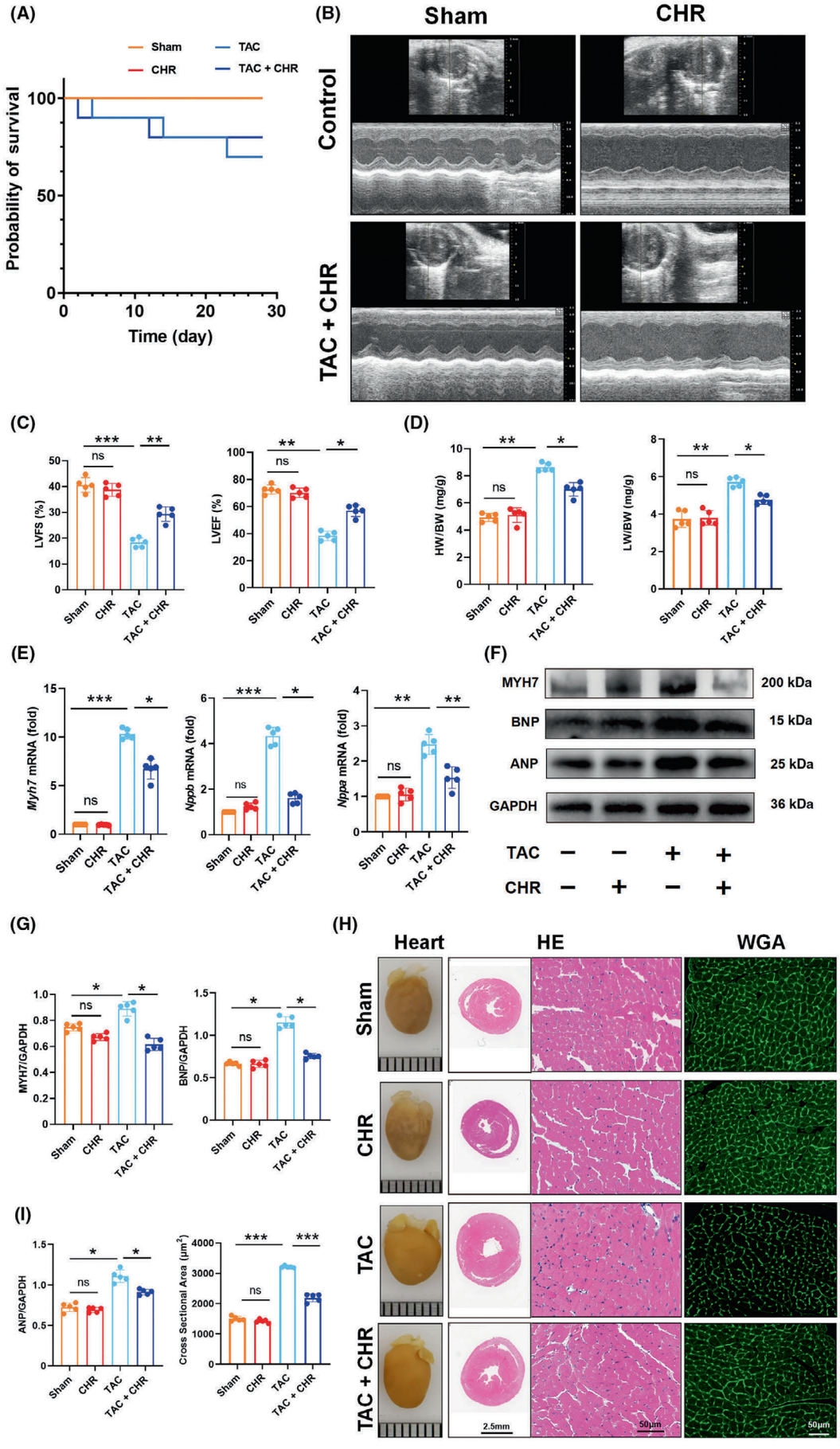
(A)
Sham
CHR
TAC
TAC + CHR
Probability of survival
Time (day)
(B)
Sham
CHR
Control
TAC + CHR
(C)
LVFS (%)
LVEF (%)
(D)
HW/BW (mg/g)
LW/BW (mg/g)
(E)
Myh7 mRNA (fold)
Nppb mRNA (fold)
Nppa mRNA (fold)
(F)
MYH7
BNP
ANP
GAPDH
200 kDa
15 kDa
25 kDa
36 kDa
TAC
CHR
(G)
MYH7/GAPDH
BNP/GAPDH
(H)
Heart
HE
WGA
(I)
ANP/GAPDH
Cross Sectional Area (μm²)
2.5mm
50μm

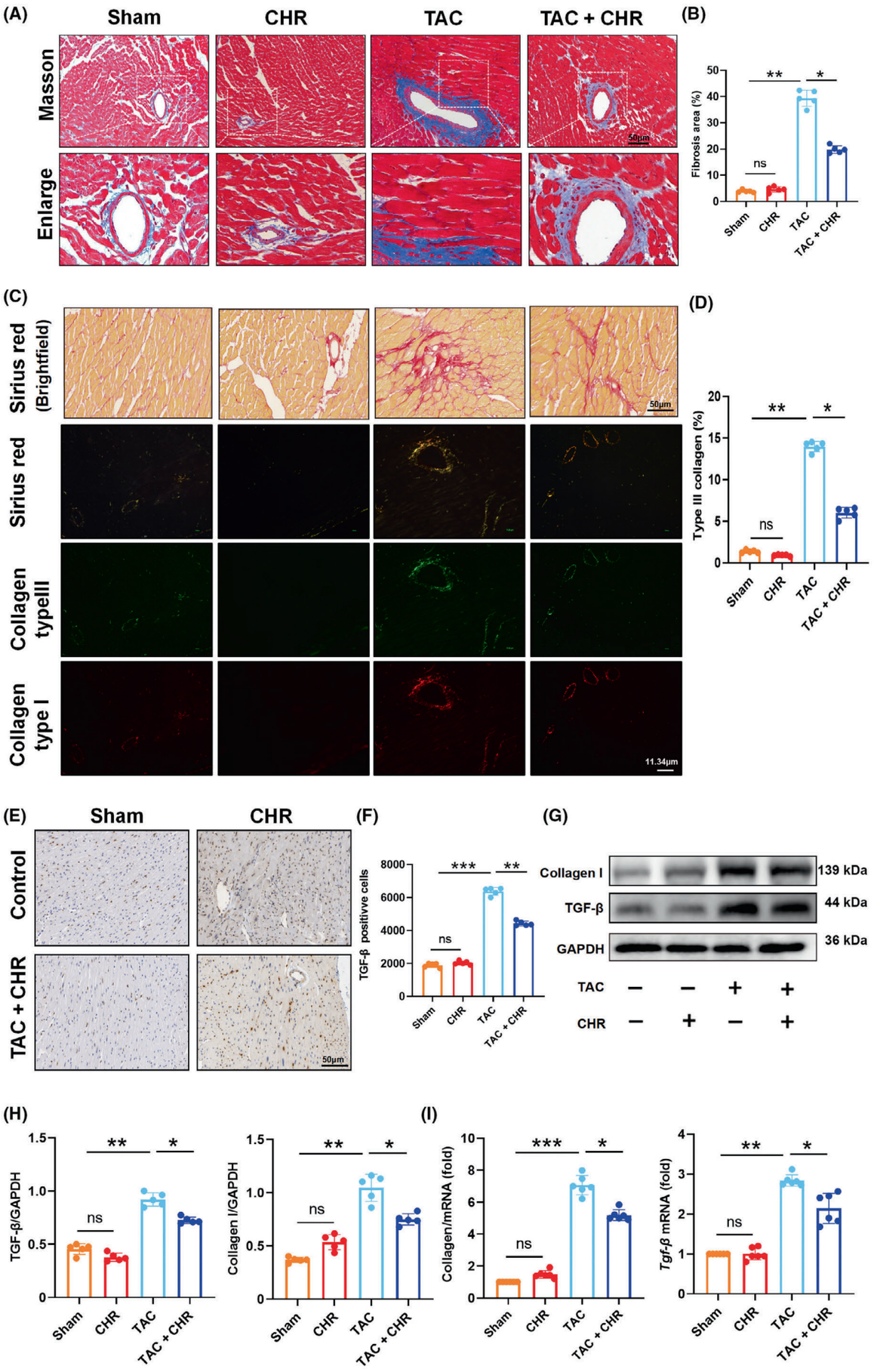
(A)
Sham
CHR
TAC
TAC + CHR
Masson
Enlarge
50μm
(B)
Fibrosis area (%)
**
*
ns
Sham
CHR
TAC
TAC + CHR
(C)
Sirius red (Brightfield)
Sirius red
Collagen typeIII
Collagen type I
50μm
11.34μm
(D)
Type III collagen (%)
**
*
ns
Sham
CHR
TAC
TAC + CHR
(E)
Sham
CHR
Control
TAC + CHR
50μm
(F)
TGF-β positivve cells
***
**
ns
Sham
CHR
TAC
TAC + CHR
(G)
Collagen I
TGF-β
GAPDH
139 kDa
44 kDa
36 kDa
TAC
CHR
(H)
TGF-β/GAPDH
Collagen I/GAPDH
**
*
ns
Sham
CHR
TAC
TAC + CHR
(I)
Collagen/mRNA (fold)
Tgf-β mRNA (fold)
***
**
*
ns
Sham
CHR
TAC
TAC + CHR

FIGURE 2 Chrysin (CHR) alleviated myocardial fibrosis of mice caused by transverse aortic constriction (TAC) surgery. (A) Masson's trichrome staining. Scale bar = 50 μm. Imaging area: Perivascular region of the left ventricle. (B) The quantitative statistics of Masson's trichrome staining. (C) Polarized light microscopy (PLM). The section orientation is transverse (5 μm thick). Scale bar = 11.34 μm. Imaging area: Perivascular region of the left ventricle. (D) Quantitative statistical analysis of collagen III proportion. (E) Immunohistochemical staining of TGF-β. Scale bar = 50 μm. Imaging area: Left ventricular anterior wall. (F) The quantitative statistics of TGF-β immunohistochemical staining. Scale bar = 50 μm. (G) The protein expression of collagen I and TGF-β using Western blot. (H) The quantitative statistics of protein bands. (I) The messenger RNA (mRNA) expression of collagen I and TGF-β using real-time polymerase chain reaction (RT-PCR). All images are from transverse sections (5 μm thick). All data are presented as mean ± SD (standard deviation). $n = 5–6$; $^{*}p < 0.05$, $^{**}p < 0.01$, and $^{***}p < 0.001$ indicate significant differences; and ns > 0.05 means no significant difference.

To define the cardioprotective efficacy of CHR on TAC surgical mice, we used Western blot to detect the expression of oxidative stress response and inflammation-related key indicators, such as superoxide dismutase 1 (SOD1), HO-1, tumor necrosis factor-α (TNF-α), and interleukin-1β (IL-1β) (Figure 3A). Results demonstrated that compared with the sham or the CHR group, the TAC group exhibited a statistical downregulation of oxidative stress response proteins SOD1 and HO-1, alongside a significant upregulation of inflammation-related proteins TNF-α and IL-1β. However, CHR administration effectively reversed these phenomena (Figure 3B). In addition, heart failure induced by pressure overload is characterized not only by the induction of pathological processes such as myocardial hypertrophy and fibrosis but also by the irreversible apoptotic events.[28] TUNEL assay was conducted to assess cardiomyocyte apoptosis in all groups (Figure 3C). Quantitative analyses demonstrated that relative to the sham or the CHR group, the amounts of TUNEL staining positive cells (green) increased significantly in the TAC group, but after CHR treatment, there was a significant reduction in TUNEL staining positive cells subjected to TAC surgery (Figure 3D). Meanwhile, RT-qPCR (Figure 3E) and Western blot (Figure 3F) were used to analyze the expression of apoptosis-related proteins such as Bcl-2 Associated X protein (BAX), cleaved-caspase-3, and B-cell lymphoma/leukemia 2 (BCL-2). Quantitative data revealed that in contrast to the sham and the CHR groups, the TAC group exhibited a statistical upregulation of the apoptotic marker cleaved-caspase-3 and BAX-to-BCL-2 ratio. Conversely, BCL-2 expression was statistically downregulated in the TAC group. Particularly, these alterations were significantly reversed after CHR treatment in mice subjected to TAC surgery (Figure 3E,G). These findings suggested that CHR exerted a potent protective effect by effectively alleviating cardiomyocyte oxidative stress, inflammatory responses, and apoptosis in mice subjected to TAC surgery.

3.4 | CHRe xertedp rotectivee ffectso n TAC surgicalm icet hrought he PI3K/AKT/NRF2p athway

To investigate CHR potential protective mechanism against myocardial remodeling, the gene expression profiles between healthy individuals and heart failure individuals with myocardial remodeling were analyzed using bioinformatics analysis. DEGs, including 1220 upregulated genes and 1063 downregulated genes, were exhibited using a volcano plot (Figure 4A). Additionally, a heat map was constructed to illustrate the relative abundance of these DEGs (Figure 4B). Based on analysis of five databases—comparative toxicogenomics database (CTD), therapeutic target database (TTD), traditional Chinese medicine systems pharmacology database and analysis platform (TCMSP), GeneCards, and DrugBank—a Venn diagram of "drug disease" revealed 164 overlapping genes associated with CHR and heart failure (Figure 4C). Protein–protein interaction network of these overlap genes highlighted 10 key target genes shared by CHR and heart failure, such as *Src*, *Akt1*, *Tnf*, *Il-6*, *Il-1β*, *Nos1*, *Calm3*, *Jun*, *Nf-κb1*, and *Esr1*, that were linked to oxidative stress and inflammatory response (Figure 4D). In addition, Kyoto Encyclopedia of Genes and Genomes (KEGG) pathway enrichment analysis was conducted on the top 35 DEGs with a *p*-value < 0.05, indicating that the PI3K/AKT signaling pathway, apoptosis, and hypertrophic cardiomyopathy were involved in significant enrichment (Figure 4E). GO enrichment analysis of biological process (Figure S2A), molecular function (Figure S2B), and cell component (Figure S2C) associated with these shared target genes was analyzed using the STRING database, further demonstrating that oxidative stress response was the crucial biological process in heart failure. We performed molecular docking between CHR and the aforementioned key common target genes using AutoDockTools, version 1.5.7. The docking results showed that the binding energies of CHR with three key target genes, *Akt1*, *Il-1β*, and *Il-6*, were − 4.82, −4.29, and − 5.99 kcal/mol, respectively (Figure S2D). A lower binding energy indicates more stable binding. Moreover, we performed Western blot to assess the expression of key proteins involved in the aforementioned finding pathway (Figure 4F). Relative to the sham or the CHR group, the ratios of p-PI3K/PI3K and p-AKT/AKT are significantly upregulated in the TAC group, and the expression level of NRF2 was significantly reduced, but CHR intervention could significantly attenuate these trends in TAC surgical mice (Figure 4G). These results implied that CHR might exert cardioprotective effects on TAC surgical mice through modulating the PI3K/AKT/NRF2 pathway.

3.5 | CHR inhibited the hypertrophy and fibrosis of ang II–treated H9C2 cells

To assess the impact of CHR on H9C2 cells treated with Ang II, we employed CCK-8 assay to explore the optimal working concentrations

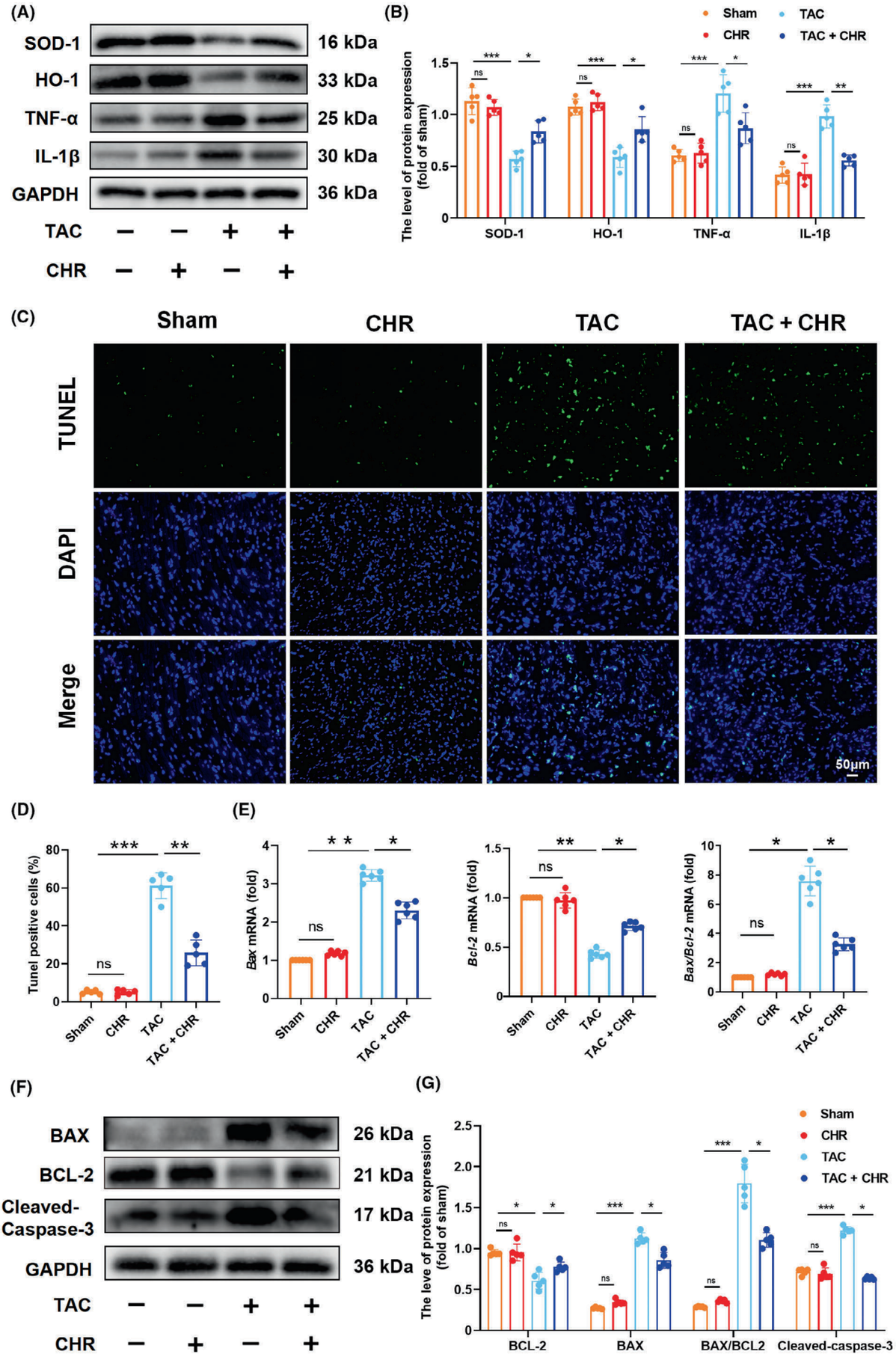
(A)
SOD-1
HO-1
TNF-α
IL-1β
GAPDH
16 kDa
33 kDa
25 kDa
30 kDa
36 kDa
TAC
CHR
(B)
Sham
CHR
TAC
TAC + CHR
The level of protein expression (fold of sham)
SOD-1
HO-1
TNF-α
IL-1β
(C)
Sham
CHR
TAC
TAC + CHR
TUNEL
DAPI
Merge
50μm
(D)
Tunel positive cells (%)
(E)
Bax mRNA (fold)
Bcl-2 mRNA (fold)
Bax/Bcl-2 mRNA (fold)
(F)
BAX
BCL-2
Cleaved-Caspase-3
GAPDH
26 kDa
21 kDa
17 kDa
36 kDa
(G)
The leve of protein expression (fold of sham)
BCL-2
BAX
BAX/BCL2
Cleaved-caspase-3

FIGURE 3 Chrysin (CHR) attenuated cardiomyocyte oxidative stress, inflammation, and apoptosis of transverse aortic constriction (TAC) surgical mice. (A) The protein expression of oxidative stress indicators superoxide dismutase 1 (SOD1) and heme oxygenase-1 (HO-1) as well as inflammatory indicators tumor necrosis factor-α (TNF-α) and interleukin-1β (IL-1β) using Western blot. (B) The quantitative statistics of these protein bands. (C) TUNEL staining in each group. Scale bar = 50 μm. Imaging area: Left ventricular anterior wall. (D) The quantitative statistics of TUNEL staining positive cells. (E) The messenger RNA (mRNA) expression of apoptotic indicators *Bax*,*B cl-2*, and *Bax/Bcl-2*. (F) The protein expression of apoptotic indicators BAX, BCL-2, and cleaved-caspase-3 using Western blot. (G) The quantitative analysis of protein bands. All images are from transverse sections (5 μm thick). All data are presented as mean ± SD (standard deviation). $n = 5–6$; $^{*}p < 0.05$, $^{**}p < 0.01$, and $^{***}p < 0.001$ indicate significant differences; and ns > 0.05 means no significant difference.

of Ang II and CHR. A gradient concentration of Ang II was used to treat H9C2 cells, and CCK-8 analysis indicated that 1000 nmol/L Ang II exerted a significant inhibitory effect on the viability of H9C2 cells (Figure S3A). Consequently, the optimal working concentration of Ang II was set as 1000 nmol/L in this study. Concurrently, the cytotoxicity of CHR at different concentrations was evaluated using CCK-8 assay, demonstrating that CHR exhibited no toxicity to H9C2 cells within the tested ranges (Figure S3B). Additionally, Ang II–treated H9C2 cells were administrated increasing doses of CHR, showing that 150-nmol/L CHR could significantly elevate the viability of Ang II–treated H9C2 cells, so this dose was chosen as the optimal working concentration of CHR (Figure S3C).

Fluorescence staining of α-actinin was employed to assess cellular hypertrophy of H9C2 cells in each group (Figure 5A), revealing that compared to the control or the CHR group, Ang II exposure led to a significant enlargement of the cross-sectional area in H9C2 cells, whereas CHR treatment significantly reduced the cell cross-sectional area in Ang II–treated H9C2 cells. Particularly, 740Y-P administration exerted a contrary effect and reversed the effect of CHR (Figure 5B). Meanwhile, we assessed the expression levels of hypertrophy-related indicators (*Myh7*, *Nppa*, and *Nppb*) and fibrosis-associated genes (*collagen I* and *Tgf-β*) in each group using RT-qPCR. The results demonstrated that these indicators significantly increased in the Ang II group relative to the control or the CHR group. However, CHR treatment partially reversed this upregulation in Ang II–treated H9C2 cells (Figure 5C). Moreover, the expression levels of hypertrophy and fibrosis markers in Ang II–exposed H9C2 cells treated with or without 740Y-P were assessed using qPCR (Figure 5D). The results showed that compared with the Ang II group, CHR treatment significantly downregulated the expression of these markers in Ang II–treated H9C2 cells, whereas 740Y-P administration exerted a contrary effect and reversed the effect of CHR. These findings further demonstrated that CHR could attenuate hypertrophy and fibrosis of Ang II–treated H9C2 cells to some extent.

3.6 | CHR mitigated oxidative stress response and inflammation of H9C2 cells treated with ang II

To assess the potential of CHR in mitigating cellular oxidative stress response and inflammation induced by Ang II, H9C2 cells were exposed to 1000 nmol/L Ang II. Immunofluorescence staining assay (Figure 6A) demonstrated that compared with the control or the CHR group, Ang II stimulation significantly inhibit the translocation of the oxidative stress factor NRF2 into the nucleus, and CHR treatment was found to promote the nucleus translocation and expression of NRF2 in Ang II–treated H9C2 cells, but this effect was particularly counteracted by the PI3K agonist 740Y-P (Figure 6B). Western blot was employed to detect the expression of the oxidative stress–related NRF2 downstream molecules SOD1 and HO-1 (Figure 6C). The assay results demonstrated that compared with the control and the CHR groups, the expression of SOD1 and HO-1 was statistically downregulated in the Ang II group. Conversely, CHR administration significantly upregulated the levels of these proteins in Ang II–exposed H9C2 cells (Figure 6D). Moreover, the expression of SOD1 and HO-1 was assessed in Ang II–treated H9C2 cells treated with or without 740Y-P using Western blot (Figure 6E). Results revealed that compared with the Ang II group, CHR treatment significantly upregulated the expression of SOD1 and HO-1 in Ang II–treated H9C2 cells, but 740Y-P administration exhibited the opposite effect and could neutralize the effect of CHR (Figure 6F). In addition, the ROS intensity of the H9C2 cells in each experimental group was examined via flow cytometry (Figure S3D). The result trend was almost consistent with the earlier result of NRF2 immunofluorescence staining (Figure S3E).

Oxidative stress response is usually accompanied by inflammatory reaction.[29] Fluorescence staining of the inflammatory factor IL-1β was performed (Figure 7A), and the expression of the inflammation-related proteins TNF-α and IL-1β was detected using Western blot in all groups (Figure 7B,C). Quantitative analyses revealed that Ang II exposure significantly elevated the levels of these inflammatory factors in contrast to the control or the CHR group, and CHR treatment could effectively ameliorate Ang II stimulation (Figure 7D,E), but 740Y-P administration could significantly offset the effect of CHR (Figure 7D,F). These data implied that CHR could attenuate oxidative stress and inflammation response in Ang II–treated H9C2 cells.

3.7 | CHR inhibited apoptosis of H9C2 cells treated witha ng II

Apoptosis is usually the ultimate event of cellular oxidative stress and inflammation.[30] Apoptosis of H9C2 cells in each experimental group was evaluated via TUNEL staining assay (Figure 8A). Results indicated that the number of apoptotic cells was almost negligible

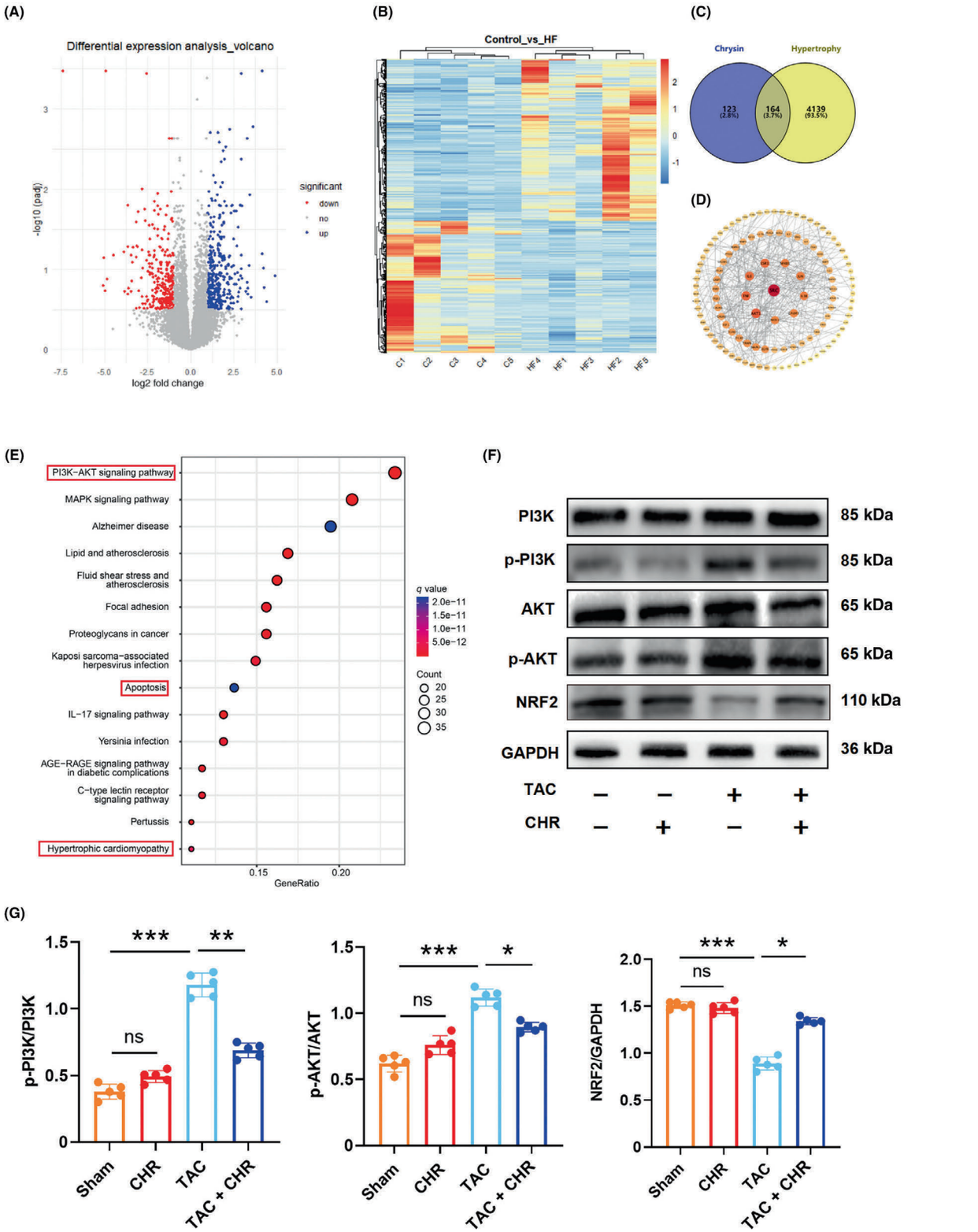

FIGURE 4 Chrysin (CHR) exerted protective effects on transverse aortic constriction (TAC) surgical mice through the PI3K/AKT-mediated nuclear factor erythroid 2-related factor 2 (NRF2) pathway. (A) A volcano plot illustrating differentially expressed genes (DEG) between healthy individuals and heart failure individuals with myocardial remodeling. (B) A heat map depicting the DEGs. (C) A Venn diagram of "drug disease" representing the overlap target genes between CHR and heart failure. (D) A protein–protein interaction (PPI) network diagram highlighting key target genes shared by CHR and heart failure. (E) Kyoto Encyclopedia of Genes and Genomes (KEGG) pathway enrichment analysis of the top 35 DEGs with p-values <0.05. (F) The expression of the PI3K/AKT pathway–related index proteins using Western blot. (G) The quantitative analysis of protein bands. All data are presented as mean ± SD (standard deviation). $n=5$; $^{*}p<0.05$, $^{**}p<0.01$, and $^{***}p<0.001$ indicate significant differences; and ns > 0.05 means no significant difference.

in the control and the CHR groups, and Ang II exposure significantly increased the positive cells (green) of TUNEL staining, but CHR treatment could effectively decrease the TUNEL staining positive cell percentage in Ang II–treated H9C2 cells, which could be counteracted by 740Y-P intervention (Figure 8B). Meanwhile, flow cytometry was conducted to detect the apoptosis rate of H9C2 cells in each group (Figure 8C). The data indicated that the apoptotic rate of H9C2 cells was relatively low in both the control and the CHR groups, and Ang II treatment significantly elevated the apoptotic rate of H9C2 cells, whereas CHR administration effectively exerted a suppressive effect on the apoptotic rate of Ang II–exposed H9C2 cells, but 740Y-P could significantly neutralize the effect of CHR (Figure 8D). Moreover, Western blot assays were performed to detect expression changes in apoptosis-related proteins among the different groups (Figure 8E,F). Quantitative analyses revealed that the expression trend of these proteins across the different groups was nearly consistent with the result of flow cytometry except for the BCL-2 level (Figure 8G,H). These data suggested that CHR could inhibit apoptosis of Ang II–treated H9C2 cells.

3.8 | CHR exerted protective functions on ang II–treated H9C2c ellst hrought he PI3K/AKT-mediated NRF2p athway

To elucidate the potential mechanism of CHR on Ang II–treated H9C2 cells, Western blot was employed to assess the expression of crucial markers implicated in the PI3K/AKT-mediated NRF2 signaling pathway, which was based on the in vivo findings mentioned earlier (Figure 9A,B). Our findings revealed that compared to the control or the CHR group, the ratios of p-PI3K/PI3K and p-AKT/AKT were significantly elevated, and the level of NRF2 was statistically decreased in Ang II–treated H9C2 cells, whereas CHR treatment significantly reversed this aforementioned trend (Figure 9C). In addition, the PI3K agonist 740Y-P could further increase the ratios of p-PI3K/PI3K and p-AKT/AKT as well as decrease the NRF2 expression in H9C2 cells treated with Ang II, and counteract the CHR function (Figure 9D). Collectively, these outcomes revealed that CHR might exert its cytoprotective effects on Ang II–treated H9C2 cells through the PI3K/AKT-mediated NRF2 pathway.

Collectively, CHR might mitigate oxidative stress response by the PI3K/AKT-mediated NRF2 pathway to reduce inflammation and apoptosis to further exert the protective effects on pressure overload–induced heart failure accompanied by myocardial hypertrophy (Figure 10).

4 | DISCUSSION

Heart failure represents a significant contributor to global mortality rates, which is characterized by ventricular hypertrophy, cardiac apoptosis, and myocardial inflammation accompanied by cardiac fibrosis, a pathological hallmark that represents the common terminal phase of diverse cardiovascular pathologies.[31–33] Myocardial remodeling, a significant risk factor for heart failure, can be induced by pressure overload that develops from the compensatory phase to the decompensatory phase.[34] Physiological myocardial remodeling does not result in heart failure, which is regarded as a normal mechanism of the body's adaptive response to physiological alterations.[35] However, pathological myocardial remodeling, induced by persistent endogenous or exogenous pressure overload, can result in heart failure.[36] The exact pathogenic mechanism underlying myocardial remodeling has not yet been fully elucidated. Therefore, it is highly significant to elucidate the underlying mechanism of pathological myocardial remodeling and to develop intervention drugs that can effectively reverse this pathological process.

A TAC model in mice or rats serves as the predominant method for developing the myocardial remodeling model, including cardiac hypertrophy accompanied by fibrosis in animals.[37] Myocardial hypertrophy and cardiac fibrosis manifest as a compensatory or adaptive response to mitigate cardiac wall stress induced by various stimulation.[38] In this study, we primarily simulated pathological myocardial remodeling induced by TAC surgery and found significant cardiac hypertrophy and fibrosis, characterized by deteriorated cardiac function, increased gross heart mass, enlarged myocardial cell volume, expanded cross-sectional area, thickened left ventricular septum and posterior wall, and accumulated fibrotic scar tissues in TAC surgical mice. The typical manifestations of pathological myocardial remodeling are two key phenotypic changes: increased heart weight and expanded cardiomyocyte volume. Then, the intensified myocardial fibrosis can cause irreversible alterations in cardiac structural remodeling and functional deterioration, which ultimately result in heart failure.[39] The heart-secreted hormones BNP and ANP are detectable when the left ventricular volume increases.[40] TGF-β can be upregulated in myocardial disorders, exerting a critical effect on cardiac remodeling through modulating the phenotypic and functional properties of cardiomyocytes.[41] CHR, a flavonoid compound mainly extracted from plant extracts, exhibits various pharmacological activities, including antioxidative, anti-inflammatory, antimutagenic, and antibacterial properties.[14,15] In our study, CHR treatment demonstrated significant enhancement of cardiac function, reduction in heart size and cross-sectional area of cardiomyocytes, suppression of cardiac wall thickness and accumulation of fibrotic scar, and downregulation of BNP, ANP, TGF-β, and collagen I expression in both TAC surgical mice and Ang II–treated H9C2 cells. This study reveals the protective role of CHR in cardiac hypertrophy models, but certain limitations still exist. As a typical flavonoid compound, CHR is characterized by low oral bioavailability and rapid in vivo metabolism[42]; although oral gavage of CHR (150 mg/kg) exhibited clear cardioprotective effects in mice, species differences in metabolic enzyme activity and gastrointestinal absorption efficiency between humans and mice may lead to insufficient

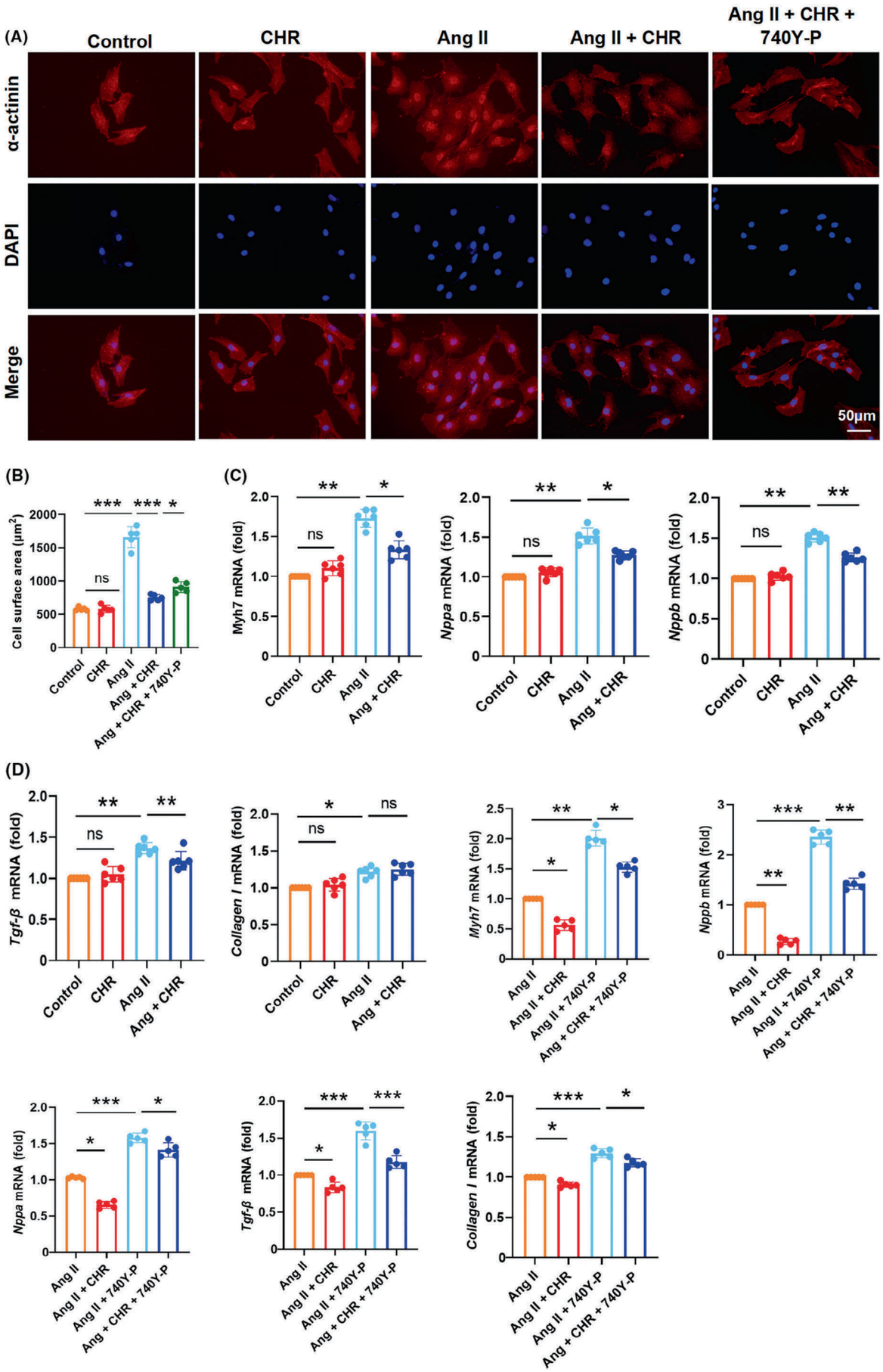
(A)
Control
CHR
Ang II
Ang II + CHR
Ang II + CHR + 740Y-P
α-actinin
DAPI
Merge
50μm
(B)
Cell surface area (μm²)
(C)
Myh7 mRNA (fold)
Nppa mRNA (fold)
Nppb mRNA (fold)
(D)
Tgf-β mRNA (fold)
Collagen I mRNA (fold)
Myh7 mRNA (fold)
Nppb mRNA (fold)
Nppa mRNA (fold)
Tgf-β mRNA (fold)
Collagen I mRNA (fold)
ns
Control
CHR
Ang II
Ang + CHR
Ang + CHR + 740Y-P
Ang II + CHR
Ang II + 740Y-P

FIGURE 5 Chrysin (CHR) inhibited the cellular hypertrophy and fibrosis of angiotensin II (Ang II)–treated H9C2 cells. (A) Immunofluorescence staining of α-actinin in each group. Scale bar = 50 μm. (B) The quantitative statistics of α-actinin expression. (C) The messenger RNA (mRNA) expression of myocardial hypertrophy indicators *Myh7*, *Nppa*, and *Nppb* as well as fibrosis indicators *Tgf-β* and *collagen I*. (D) The mRNA expression of myocardial hypertrophy indicators *Myh7*, *Nppa*, and *Nppb* as well as fibrosis indicators *Tgf-β* and *collagen I* in angiotensin II (Ang II)–exposed H9C2 cells treated with or without 740Y-P. All data are presented as mean ± SD (standard deviation). $n = 5–6$; $^{*}p < 0.05$, $^{**}p < 0.01$, and $^{***}p < 0.001$ indicate significant differences; and ns > 0.05 means no significant difference.

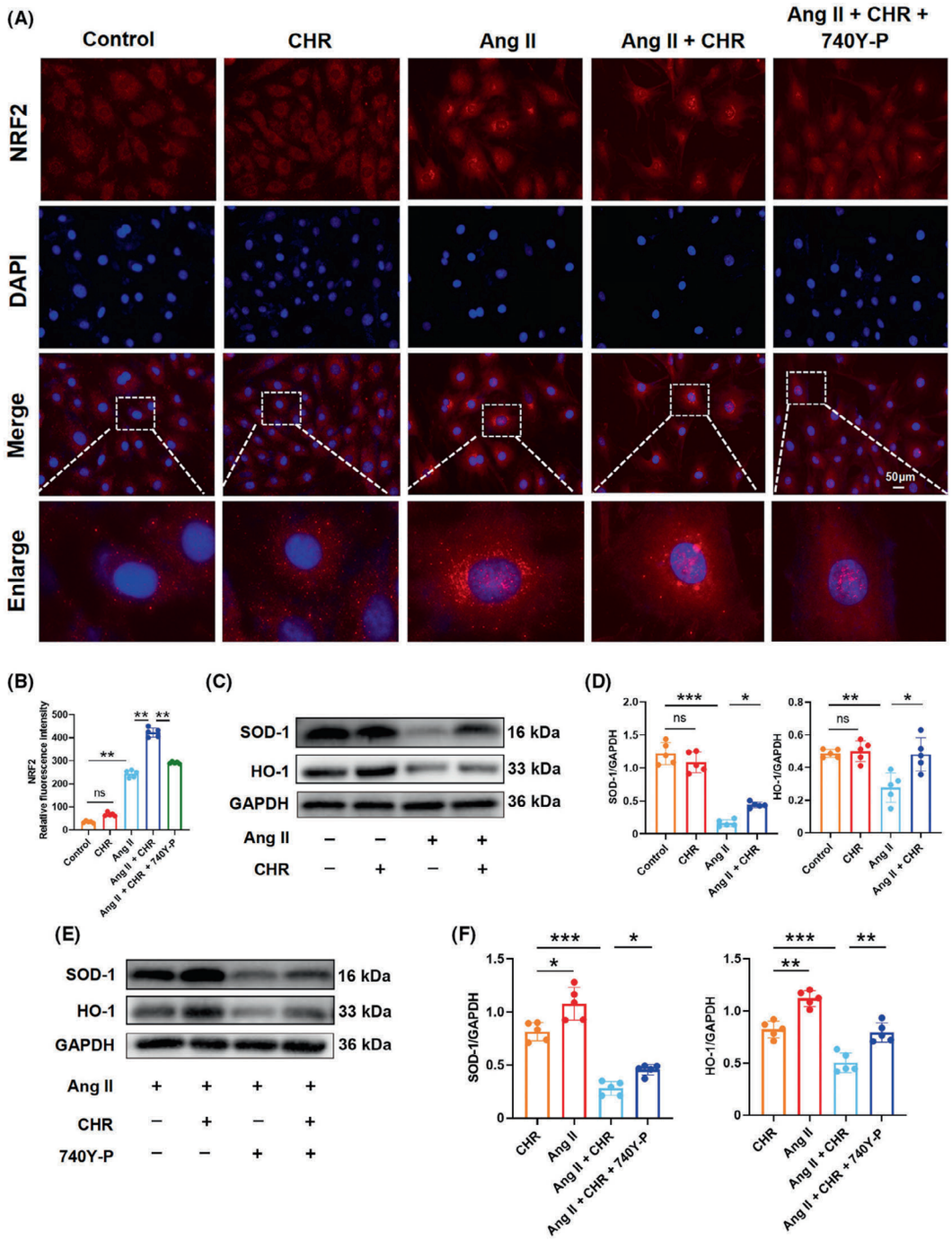

FIGURE 6 Chrysin (CHR) mitigated oxidative stress response of angiotensin II (Ang II)–treated H9C2 cells. (A) Immunofluorescence staining of nuclear factor erythroid 2-related factor 2 (NRF2) in each group. Scale bar = 50 μm. (B) The quantitative statistics of NRF2 expression. (C) The protein expression of oxidative stress indicators superoxide dismutase 1 (SOD1) and heme oxygenase-1 (HO-1) using Western blot. (D) The quantitative statistics of protein bands. (E) The protein expression of oxidative stress indicators SOD1 and HO-1 in Ang II–exposed H9C2 cells treated with or without 740Y-P was analyzed using Western blot. (F) The quantitative statistics of protein bands. All data are presented as mean ± SD (standard deviation). $n = 5$; $^{*}p < 0.05$, $^{**}p < 0.01$, and $^{***}p < 0.001$ indicate significant differences; and ns > 0.05 means no significant difference.

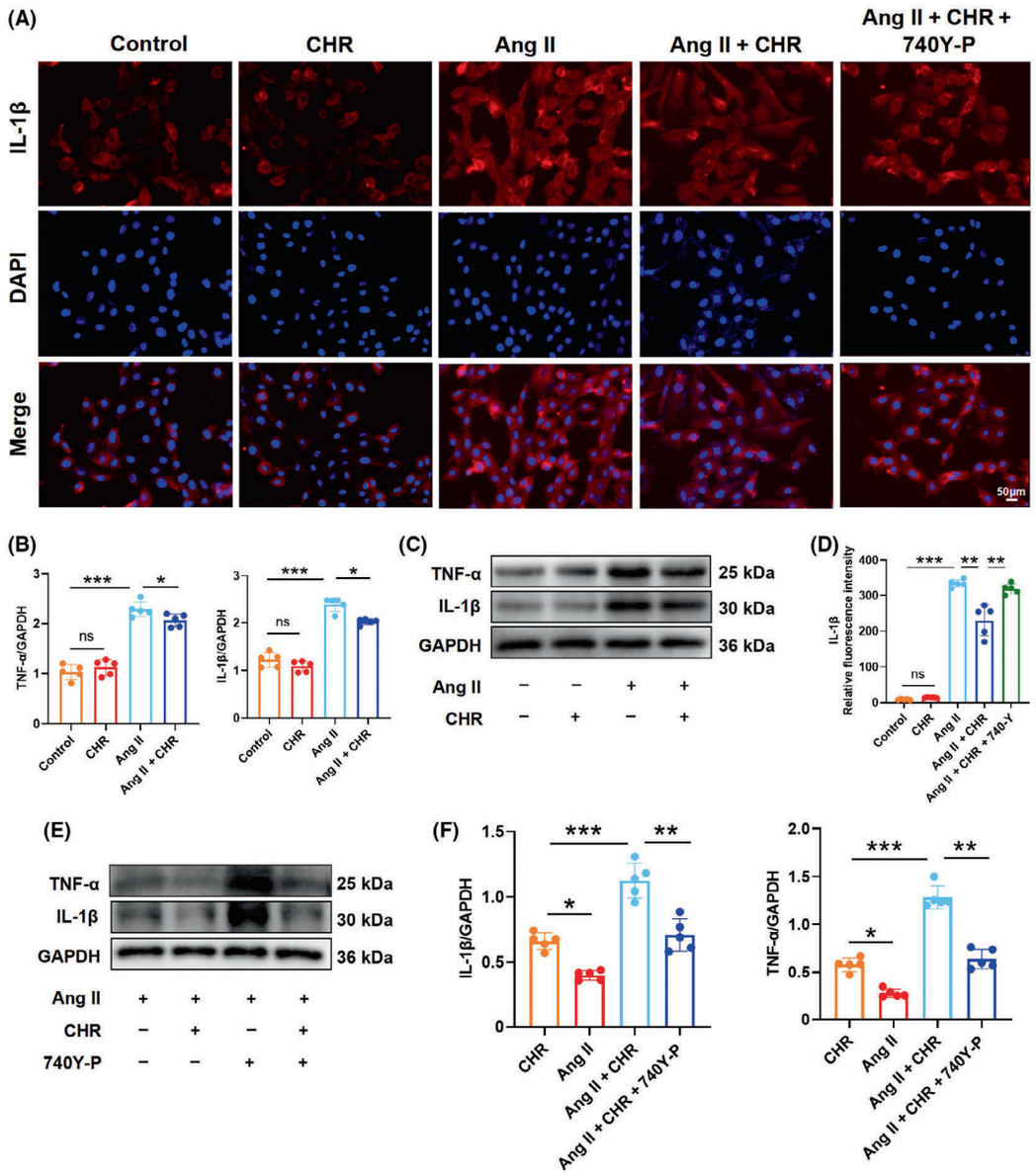

FIGURE 7 Chrysin (CHR) alleviated inflammation of angiotensin II (Ang II)–treated H9C2 cells. (A) Immunofluorescence staining of interleukin-1β (IL-1β) in each group. Scale bar = 50 μm. (B) The protein expression of inflammatory indicators tumor necrosis factor-α (TNF-α) and IL-1β using Western blot. (C) The protein expression of inflammatory indicators TNF-α and IL-1β in Ang II–exposed H9C2 cells treated with or without 740Y-P using Western blot. (D) The quantitative statistics of IL-1β expression. (E) The quantitative statistics of protein bands. (F) The quantitative statistics of protein bands. All data are presented as mean ± SD (standard deviation). $n = 5$; $^{*}p < 0.05$, $^{**}p < 0.01$, and $^{***}p < 0.001$ indicate significant differences; and ns > 0.05 means no significant difference.

CHR concentrations in human myocardial tissue at the same dose, potentially compromising its therapeutic efficacy in clinical translation. Future research should incorporate nanoformulation techniques to improve its bioavailability.[42]

Myocardial remodeling is associated with the disruption of cardiomyocyte homeostasis, encompassing oxidative stress response, cellular inflammation, and apoptosis.[43] Our finding supported the antioxidative role of CHR in TAC surgical mice, which was consistent with prior research, indicating that CHR had the cytoprotective effects against aluminum phosphide–mediated myocardial toxicity in rat by modulation of oxidative stress response.[44] Prolonged stress on the heart can result in increased oxygen consumption by myocardial cells, which subsequently triggers a state of relative hypoxia, leading to the interruption of energy metabolism and the leakage of mitochondrial ROS.[45,46] In this study, we detected the increase in ROS levels as well as the decrease in SOD1 and HO-1 levels in TAC surgical mice and Ang II–stimulated H9C2 cells, which were significantly reversed after CHR intervention. Antioxidant enzymes such as SOD1 and HO-1 are integral to the catalysis of superoxide free radicals and

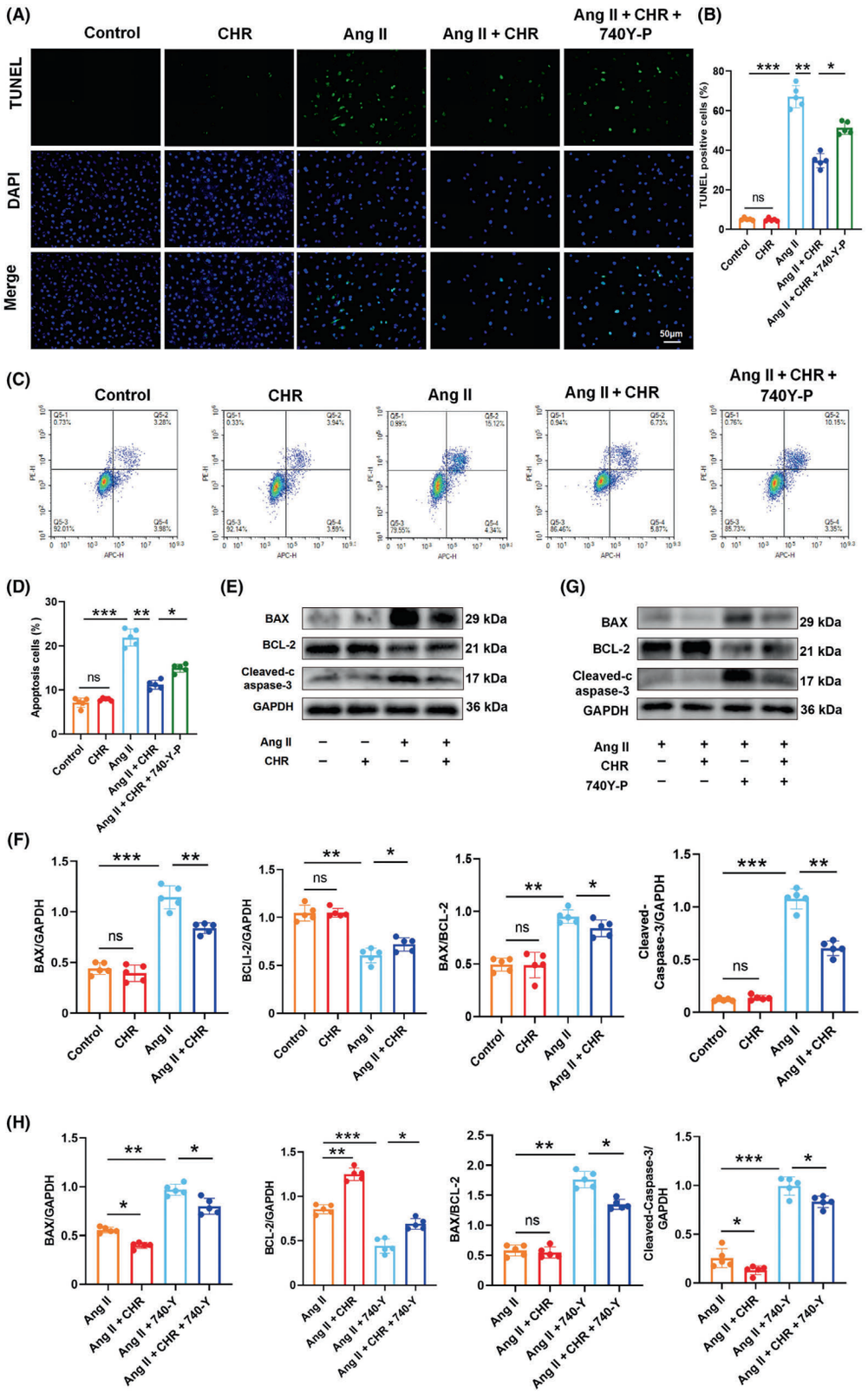

FIGURE 8 Chrysin (CHR) inhibited cell apoptosis of angiotensin II (Ang II)–treated H9C2 cells. (A) TUNEL staining of H9C2 cells in each group. Scale bar = 50 μm. (B) The quantitative statistics of TUNEL staining. (C) Detection of the apoptosis rate of cells using flow cytometry in each group. (D) The statistical analysis of apoptosis rate. (E) The protein expression of apoptosis-related proteins BAX, BCL-2, and cleaved-caspase-3 using Western blot. (F) The protein expression of apoptosis-related proteins BAX, BCL-2, and cleaved-caspase-3 using Western blot. (G) The quantitative statistics of protein bands. (H) The quantitative statistics of protein bands. All data are presented as mean ± SD (standard deviation). $n = 3–5$; $^{*}p < 0.05$, $^{**}p < 0.01$, and $^{***}p < 0.001$ indicate significant differences; and ns > 0.05 means no significant difference.

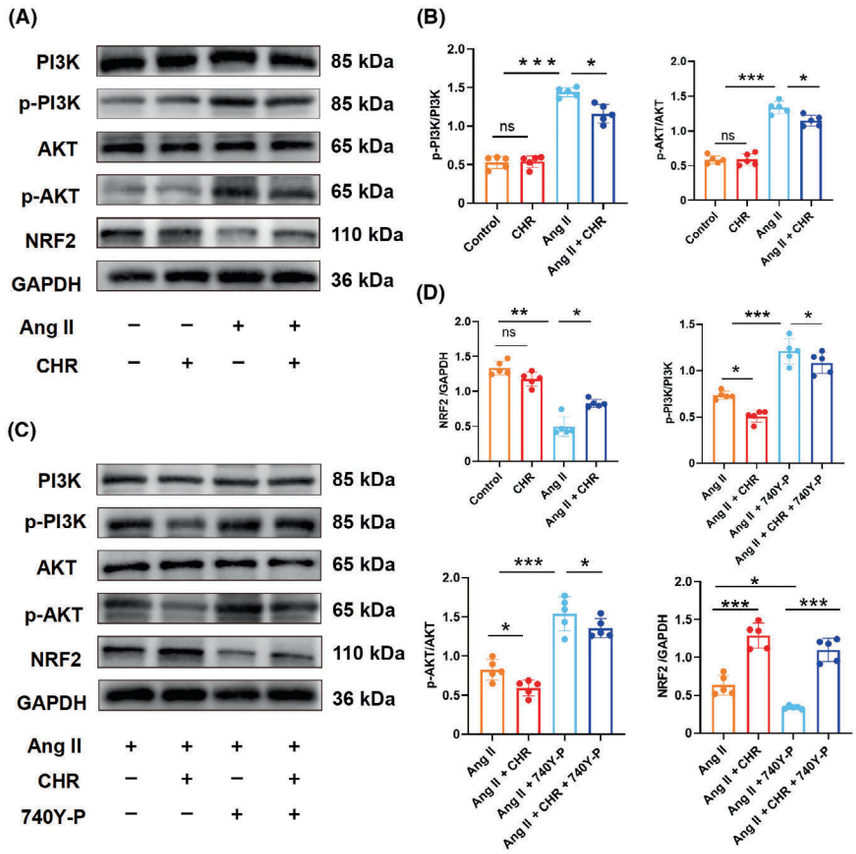

FIGURE 9 Chrysin (CHR) exerted protective effects on angiotensin II (Ang II)–treated H9C2 cells through the PI3K/AKT-mediated nuclear factor erythroid 2-related factor 2 (NRF2) pathway. (A) The protein expression of the PI3K/AKT-mediated NRF2 pathway such as PI3K, p-PI3K, AKT, p-AKT, and NRF2 in different groups using Western blot. (C) The quantitative statistics of protein bands. (B) The expression of PI3K, p-PI3K, AKT, p-AKT, and NRF2 proteins in different groups using Western blot. (D) The quantitative statistics of protein bands. All data are presented as mean ± SD (standard deviation). $n = 5$; $^{*}p < 0.05$, $^{**}p < 0.01$, and $^{***}p < 0.001$ indicate significant differences; and ns > 0.05 means no significant difference.

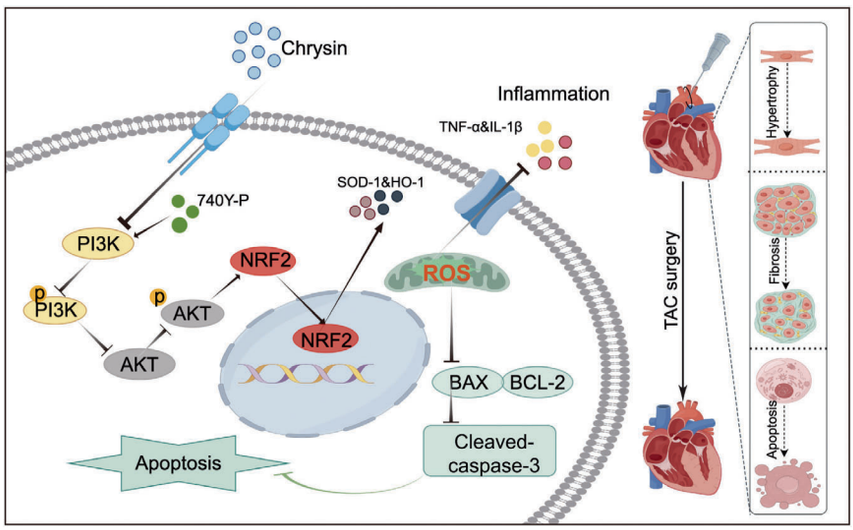

FIGURE 10 Schematic diagram of the potential effect mechanism of chrysin (CHR) on pressure overload–induced myocardial remodeling.

peroxides, thereby constituting the core of the body's antioxidant defense system and mitigating tissue damage associated with oxidative stress.[47] Ginsenoside Rd., a major bioactive component of ginsenosides, has been demonstrated to attenuate cardiac hypertrophy induced by TAC surgery via the suppression of oxidative stress.[38]

Oxidative stress response is considered as a pivotal pathological process, which contributes to inflammation and apoptosis of cardiomyocytes in chronic heart failure.[48] Cardiomyocytes are responsible for electrical conduction and cardiac contraction, and are integral to the maintenance of metabolic equilibrium and cardiac pumping function.[49] Previous research has demonstrated that after TAC surgery, the release of pro-inflammatory indicators such as TNF-α and IL-1β facilitated the infiltration of inflammatory cells into the myocardial tissues.[50] The present study also identified significant upregulation of these inflammatory factors in TAC surgical mice and Ang II–treated H9C2 cells. It is worth noting that this upregulation was substantially reversed after treatment with CHR.

In addition, the induction of cardiomyocyte apoptosis is a critical driver for the occurrence and progression of heart failure.[51] Inhibiting cardiomyocyte apoptosis can effectively enhance the survival rate of heart failure patients while mitigating ventricular remodeling and dysfunction.[52] In this study, TUNEL staining was employed to detect cellular apoptosis, demonstrating that CHR significantly attenuated apoptosis in both TAC surgical mice and Ang II–stimulated H9C2 cells. Apoptosis is initiated via the endogenous apoptotic pathway, which is triggered by the activation of intracellular signals, including BAX, BCL-2, and cytochrome C.[53] Upon release into the cytoplasm, these signals initiate the caspase cascade, involving the sequential activation of caspase-9 and caspase-3, ultimately leading to DNA fragmentation and chromatin condensation, thereby exerting a pivotal role in the modulation of apoptotic processes.[54] Our study confirmed that CHR significantly upregulated BCL-2, simultaneously downregulated BAX and cleaved-caspase-3, and reduced the proportion of apoptotic cells, thus inhibiting apoptosis in TAC surgical mice and Ang II–stimulated H9C2.

To elucidate the underlying protective mechanism of CHR in alleviating myocardial remodeling, the gene expression profiles between healthy individuals and heart failure patients with myocardial remodeling were analyzed using bioinformatics analysis, and the key protein expression in the crucial pathway was further verified using Western blot. We found that there were 10 key target genes shared by CHR and heart failure, namely *Src*, *Akt1*, *Tnf*, *Il-6*, *Il-1β*, *Nos1*, *Calm3*, *Jun*, *Nf-κb1*, and *Esr*1, which were associated with oxidative stress response and inflammation reaction.[55] Furthermore, the PI3K/AKT signaling pathway, apoptosis, and hypertrophic cardiomyopathy were defined as critical contributors to the pathogenesis of heart failure via KEGG pathway enrichment analysis. Particularly, the PI3K/AKT signaling pathway has been confirmed to be a mediator of oxidative stress, inflammation, and apoptosis, which are critical physiological processes involved in diverse diseases.[56,57] Prior studies have found that the PI3K/AKT signaling pathway could mitigate stress overload–induced myocardial remodeling and heart failure.[19] Besides, the PI3K/AKT signaling pathway is implicated in the modulation of inflammatory responses.[58]

The PI3K/AKT pathway is an important upstream regulator of NRF2, a master regulator of the antioxidant response.[11,58] A previous report has indicated that TRIM26 overexpression suppresses the PI3K/AKT pathway activation, and administration of the PI3K agonist 740Y-P can abrogate the antitumor activity of TRIM26 in PTC cells.[59] NRF2 is a pivotal regulator in the body's response to oxidative stress.[60] Particularly, our study confirmed that CHR could significantly reverse the elevated p-PI3K/PI3K and p-AKT/AKT ratios in both TAC surgical mice and Ang II–treated H9C2 cells. The compound 740Y-P is known to modulate the PI3K/AKT pathway.[59] Our results revealed that the antioxidative, anti-inflammatory, and antiapoptotic effects of CHR could be almost abrogated by 740Y-P treatment, suggesting that CHR might exert protective effects against TAC surgical mice and Ang II–treated H9C2 cells through modulating the PI3K/AKT-mediated NRF2 pathway. Additionally, other research studies have demonstrated that oxidative stress led to an increase in ROS level, which in turn triggered the PI3K/AKT signaling cascade, and subsequently activated the NRF2 receptor.[61] Relevant studies have shown that the PI3K/AKT/NRF2 pathway can achieve cross-regulation with other myocardial remodeling-related pathways (e.g., mitogen-activated protein kinase [MAPK] and nuclear factor kappa B [NF-κB]).[62–64] It is speculated that CHR may exert its effects through the synergistic action of multiple pathways. For example, the NF-κB pathway, as a core regulatory pathway of inflammatory responses, can be activated by oxidative stress, whereas NRF2 and NF-κB exhibit a mutually inhibitory regulatory relationship.[65,66] It is hypothesized that CHR may indirectly inhibit NF-κB pathway activity by activating NRF2, thereby further enhancing its anti-inflammatory effects. However, this hypothesis still requires experimental validation in future studies. Furthermore, MAPK pathways (e.g., p38 MAPK and extracellular signal-regulated kinase 1/2) are involved in pressure overload–induced myocardial hypertrophy and fibrosis.[67] Whether CHR regulates these pathways and whether it exhibits synergistic or antagonistic interactions with the PI3K/AKT/NRF2 pathway warrant further investigation.

Certainly, our current study still has several limitations that need to be addressed in future studies. First, we did not conduct in vivo rescue experiments to further confirm the protective mechanism of CHR in TAC surgical mice. Transgenic mice with conditional knockout of key target genes should be introduced in future studies. Second, the in vitro experiments did not employ primary cardiomyocytes, which would provide more convincing evidence. Third, the therapeutic effect of CHR on pressure overload–related cardiac dysfunction, myocardial remodeling, and even heart failure should be verified in future clinical studies. Fourth, the therapeutic efficacy of CHR in cardiac dysfunction associated with pressure overload–induced myocardial remodeling and even heart failure requires validation through future clinical research. For instance, there is an immediate need to conduct integrated pharmacokinetic and pharmacodynamic studies in larger animal models (e.g., pigs) to verify target organ exposure and therapeutic effects, thereby providing critical preclinical data to support its eventual translation to clinical trials.

Although the mechanism mediating the pathological changes responsible for myocardial remodeling has not been fully elucidated, our present study revealed that CHR might exert protective effects against pressure overload–induced myocardial remodeling through modulating the PI3K/AKT/NRF2 pathway–mediated oxidative stress response to alleviate myocardial cell inflammation and apoptosis, suggesting that CHR may be a promising therapeutic agent for pressure overload–induced cardiac diseases.

AUTHOR CONTRIBUTIONS

Yijia Wang: Methodology; writing – original draft. **Xing Feng:** Conceptualization; writing – original draft. **Shuhui Zhao:** Conceptualization; data curation; writing – original draft. **Yuchong Fu:** Software; validation. **Ao Zhang:** Methodology. **Xiaofeng Shen:** Methodology; validation. **Bowen Yu:** Formal analysis; investigation. **Yihao Wang:** Validation. **Jiahui Lin:** Validation. **Bing Zhang:** Investigation. **Weiping Ji:** Funding acquisition. **Lianpin Wu:** Funding acquisition. **Xiaoling Guo:** Funding acquisition; writing – original draft; writing – review and editing.

ACKNOWLEDGMENTS

The author have nothing to report.

FUNDING INFORMATION

This study received funding from the Key Research and Development Program of Zhejiang Province (2023C03018), the Natural Science Foundation of Zhejiang Province (LY24H020008), and the Jie Bang Gua Shuai Project of the Wenzhou Science and Technology Bureau (ZY2023022 and ZY2024019).

CONFLICT OF INTEREST STATEMENT

The authors state that no financial interests or personal relationships exist that could have influenced the work presented in this paper.

ETHICS STATEMENT

All experiments were approved by the Animal Ethics Committee at the Wenzhou Institute, University of Chinese Academy of Sciences (WIUCAS24062701). All procedures followed ethical standards for animal research in strict accordance with the Guide for the Care and Use of Laboratory Animals.

ORCID

Xiaoling Guo https://orcid.org/0009-0002-3483-2115

REFERENCES

1. Shah AM, Claggett B, Sweitzer NK, et al. Cardiac structure and function and prognosis in heart failure with preserved ejection fraction: findings from the echocardiographic study of the treatment of preserved cardiac function heart failure with an aldosterone antagonist (TOPCAT) trial. *Circ Heart Fail*. 2014;7:740-751. doi:10.1161/CIRCHEARTFAILURE.114.001583
2. Creemers EE, Pinto YM. Molecular mechanisms that control interstitial fibrosis in the pressure-overloaded heart. *Cardiovasc Res*. 2011;89:265-272. doi:10.1093/cvr/cvq308
3. Okin PM, Devereux RB, Liu JE, et al. Regression of electrocardiographic left ventricular hypertrophy predicts regression of echocardiographic left ventricular mass: the LIFE study. *J Hum Hypertens*. 2004;18:403-409. doi:10.1038/sj.jhh.1001707
4. Ritsinger V, Nyström T, Saleh N, Lagerqvist B, Norhammar A. Heart failure is a common complication after acute myocardial infarction in patients with diabetes: a nationwide study in the SWEDEHEART registry. *Eur J Prev Cardiol*. 2020;27:1890-1901. doi:10.1177/2047487319901063
5. Kochar A, Doll JA, Liang L, Curran J, Peterson ED. Temporal trends in post myocardial infarction heart failure and outcomes among older adults. *J Card Fail*. 2022;28:531-539. doi:10.1016/j.cardfail.2021.09.001
6. Wu Y, Huang X, He Y, et al. Mechanism of puerarin alleviating myocardial remodeling through NSUN2-mediated m5C methylation modification. *Phytomedicine*. 2025;143:156849. doi:10.1016/j.phymed.2025.156849
7. Bai W, Ren M, Cheng W, Lu X, Liu D, Wang B. Qindan capsule attenuates myocardial hypertrophy and fibrosis in pressure overload-induced mice involving mTOR and TGF-β1/Smad signaling pathway inhibition. *Evid Based Complement Alternat Med*. 2021;2021:5577875. doi:10.1155/2021/5577875
8. Frangogiannis NG. The extracellular matrix in ischemic and nonischemic heart failure. *Circ Res*. 2019;125:117-146. doi:10.1161/CIRCRESAHA.119.311148
9. Messerli FH, Rimoldi SF, Bangalore S. The transition from hypertension to heart failure: contemporary update. *JACC Heart Fail*. 2017;5:543-551. doi:10.1016/j.jchf.2017.04.012
10. Abdellatif SY, Fares NH, Elsharkawy SH, Mahmoud YI. Calanus oil attenuates isoproterenol-induced cardiac hypertrophy by regulating myocardial remodeling and oxidative stress. *Ultrastruct Pathol*. 2023;47:12-21. doi:10.1080/01913123.2022.2163016
11. Yoon JH, Youn K, Jun M. Protective effect of sargahydroquinoic acid against aβ(25-35)-evoked damage via PI3K/Akt mediated Nrf2 antioxidant defense system. *Biomed Pharmacother*. 2021;144:112271. doi:10.1016/j.biopha.2021.112271
12. Loboda A, Damulewicz M, Pyza E, Jozkowicz A, Dulak J. Role of Nrf2/HO-1 system in development, oxidative stress response and diseases: an evolutionarily conserved mechanism. *Cell Mol Life Sci*. 2016;73:3221-3247. doi:10.1007/s00018-016-2223-0
13. Patel RV, Mistry B, Syed R, et al. Chrysin-piperazine conjugates as antioxidant and anticancer agents. *Eur J Pharm Sci*. 2016;88:166-177. doi:10.1016/j.ejps.2016.02.011
14. Zeinali M, Rezaee SA, Hosseinzadeh H. An overview on immunoregulatory and anti-inflammatory properties of chrysin and flavonoids substances. *Biomed Pharmacother*. 2017;92:998-1009. doi:10.1016/j.biopha.2017.06.003
15. Mani R, Natesan V. Chrysin: sources, beneficial pharmacological activities, and molecular mechanism of action. *Phytochemistry*. 2018;145:187-196. doi:10.1016/j.phytochem.2017.09.016
16. Naz S, Imran M, Rauf A, et al. Chrysin: pharmacological and therapeutic properties. *Life Sci*. 2019;235:116797. doi:10.1016/j.lfs.2019.116797
17. Li TF, Ma J, Han XW, et al. Chrysin ameliorates cerebral ischemia/reperfusion (I/R) injury in rats by regulating the PI3K/Akt/mTOR pathway. *Neurochem Int*. 2019;129:104496. doi:10.1016/j.neuint.2019.104496
18. Xingyue L, Shuang L, Qiang W, Jinjuan F, Yongjian Y. Chrysin ameliorates sepsis-induced cardiac dysfunction through upregulating Nfr2/heme oxygenase 1 pathway. *J Cardiovasc Pharmacol*. 2021;77:491-500. doi:10.1097/FJC.0000000000000989
19. Zhang T, Li L, Mo X, et al. Matairesinol blunts adverse cardiac remodeling and heart failure induced by pressure overload by regulating Prdx1 and PI3K/AKT/FOXO1 signaling. *Phytomedicine*. 2024;135:156054. doi:10.1016/j.phymed.2024.156054

20. Lim W, Ryu S, Bazer FW, Kim SM, Song G. Chrysin attenuates progression of ovarian cancer cells by regulating signaling cascades and mitochondrial dysfunction. *J Cell Physiol*. 2018;233:3129-3140. doi:10.1002/jcp.26150
21. Zhao D, Zhong G, Li J, et al. Targeting E3 ubiquitin ligase WWP1 prevents cardiac hypertrophy through destabilizing DVL2 via inhibition of K27-linked ubiquitination. *Circulation*. 2021;144:694-711. doi:10.1161/CIRCULATIONAHA.121.054827
22. Morán MA, Gómez-Ramos P. Cholinesterase histochemistry in the human brain: effect of various fixation and storage conditions. *J Neurosci Methods*. 1992;43:49-54. doi:10.1016/0165-0270(92)90066-M
23. Guan Y, Ruan J, Tan P, et al. Hesperidin alleviates endothelial cell inflammation and apoptosis of Kawasaki disease through inhibiting the TLR4/IκBα/NF-κB pathway. *Chem Biol Interact*. 2025;411:111445. doi:10.1016/j.cbi.2025.111445
24. Chi M, Liu J, Mei C, et al. TEAD4 functions as a prognostic biomarker and triggers EMT via PI3K/AKT pathway in bladder cancer. *J Exp Clin Cancer Res*. 2022;41:175. doi:10.1186/s13046-022-02377-3
25. Shang J, Jiao J, Yan M, et al. Chrysin protects against cerebral ischemia-reperfusion injury in hippocampus via restraining oxidative stress and transition elements. *Biomed Pharmacother*. 2023;161:114534. doi:10.1016/j.biopha.2023.114534
26. Soliman MM, Aldhahrani A, Ghamry HI, et al. Chrysin abrogates gibberellic acid-induced testicular oxidative stress and dysfunction via the regulation of antioxidants and steroidogenesis- and apoptosis-associated genes. *J Food Biochem*. 2022;46:e14165. doi:10.1111/jfbc.14165
27. Yuan L, Bu S, du M, et al. RNF207 exacerbates pathological cardiac hypertrophy via post-translational modification of TAB1. *Cardiovasc Res*. 2023;119:183-194. doi:10.1093/cvr/cvac039
28. Liu X, Li H, Hastings MH, et al. miR-222 inhibits pathological cardiac hypertrophy and heart failure. *Cardiovasc Res*. 2024;120:262-272. doi:10.1093/cvr/cvad184
29. Lin Y, Jiang M, Chen W, Zhao T, Wei Y. Cancer and ER stress: mutual crosstalk between autophagy, oxidative stress and inflammatory response. *Biomed Pharmacother*. 2019;118:109249. doi:10.1016/j.biopha.2019.109249
30. Lan X, Zhao J, Zhang Y, Chen Y, Liu Y, Xu F. Oxymatrine exerts organ- and tissue-protective effects by regulating inflammation, oxidative stress, apoptosis, and fibrosis: from bench to bedside. *Pharmacol Res*. 2020;151:104541. doi:10.1016/j.phrs.2019.104541
31. Wang B, Yang Q, Bai WW, et al. Tongxinluo protects against pressure overload-induced heart failure in mice involving VEGF/Akt/eNOS pathway activation. *PLoS One*. 2014;9:e98047. doi:10.1371/journal.pone.0098047
32. Chen X, Zhang Z, Zhang X, et al. Paeonol attenuates heart failure induced by transverse aortic constriction via ERK1/2 signaling. *Pharm Biol*. 2022;60:562-569. doi:10.1080/13880209.2022.2040543
33. Alcaide P, Kallikourdis M, Emig R, Prabhu SD. Myocardial inflammation in heart failure with reduced and preserved ejection fraction. *Circ Res*. 2024;134:1752-1766. doi:10.1161/CIRCRESAHA.124.323659
34. Cohn JN, Ferrari R, Sharpe N. Cardiac remodeling--concepts and clinical implications: a consensus paper from an international forum on cardiac remodeling. Behalf of an international forum on cardiac remodeling. *J Am Coll Cardiol*. 2000;35:569-582. doi:10.1016/s0735-1097(99)00630-0
35. Shimizu I, Minamino T. Physiological and pathological cardiac hypertrophy. *J Mol Cell Cardiol*. 2016;97:245-262. doi:10.1016/j.yjmcc.2016.06.001
36. Zhao L, Cheng G, Choksi K, et al. Transplantation of human umbilical cord blood-derived cellular fraction improves left ventricular function and remodeling after myocardial ischemia/reperfusion. *Circ Res*. 2019;125:759-772. doi:10.1161/CIRCRESAHA.119.315216
37. Bosch L, de Haan JJ, Bastemeijer M, et al. The transverse aortic constriction heart failure animal model: a systematic review and meta-analysis. *Heart Fail Rev*. 2021;26:1515-1524. doi:10.1007/s10741-020-09960-w
38. Zhang N, An X, Lang P, Wang F, Xie Y. Ginsenoside Rd contributes the attenuation of cardiac hypertrophy in vivo and in vitro. *Biomed Pharmacother*. 2019;109:1016-1023. doi:10.1016/j.biopha.2018.10.081
39. Khouri MG, Peshock RM, Ayers CR, de Lemos JA, Drazner MH. A 4-tiered classification of left ventricular hypertrophy based on left ventricular geometry: the Dallas heart study. *Circ Cardiovasc Imaging*. 2010;3:164-171. doi:10.1161/CIRCIMAGING.109.883652
40. Mendes P, Martinho R, Leite S, et al. Chronic exercise induces pathological left ventricular hypertrophy in adrenaline-deficient mice. *Int J Cardiol*. 2018;253:113-119. doi:10.1016/j.ijcard.2017.10.014
41. Frangogiannis NG. Transforming growth factor-β in myocardial disease. *Nat Rev Cardiol*. 2022;19:435-455. doi:10.1038/s41569-021-00646-w
42. Qu Y, Mu S, Song C, Zheng G. Preparation and in vitro/in vivo evaluation of a self-microemulsifying drug delivery system containing chrysin. *Drug Dev Ind Pharm*. 2021;47:1127-1139. doi:10.1080/03639045.2021.1988092
43. Meng X, Li Y, Meng L, et al. Growth differentiation factor 15 inhibits cardiac fibrosis, oxidative stress, inflammation, and apoptosis in a rat model of heart failure with preserved ejection fraction. *Front Biosci (Landmark Ed)*. 2025;30:26857. doi:10.31083/FBL26857
44. Khezri S, Sabzalipour T, Jahedsani A, Azizian S, Atashbar S, Salimi A. Chrysin ameliorates aluminum phosphide-induced oxidative stress and mitochondrial damages in rat cardiomyocytes and isolated mitochondria. *Environ Toxicol*. 2020;35:1114-1124. doi:10.1002/tox.22947
45. Akhmedov AT, Rybin V, Marín-García J. Mitochondrial oxidative metabolism and uncoupling proteins in the failing heart. *Heart Fail Rev*. 2015;20:227-249. doi:10.1007/s10741-014-9457-4
46. Takimoto E, Champion HC, Li M, et al. Oxidant stress from nitric oxide synthase-3 uncoupling stimulates cardiac pathologic remodeling from chronic pressure load. *J Clin Invest*. 2005;115:1221-1231. doi:10.1172/JCI21968
47. Shie PH, Huang SS, Deng JS, Huang GJ. Spiranthes sinensis suppresses production of pro-inflammatory mediators by Down-regulating the NF-κB signaling pathway and up-regulating HO-1/Nrf2 anti-oxidant protein. *Am J Chin Med*. 2015;43:969-989. doi:10.1142/S0192415X15500561
48. Distefano G, Sciacca P. Molecular pathogenesis of myocardial remodeling and new potential therapeutic targets in chronic heart failure. *Ital J Pediatr*. 2012;38:41. doi:10.1186/1824-7288-38-41
49. Cai K, Jiang H, Zou Y, et al. Programmed death of cardiomyocytes in cardiovascular disease and new therapeutic approaches. *Pharmacol Res*. 2024;206:107281. doi:10.1016/j.phrs.2024.107281
50. Kim HJ, Park KG, Yoo EK, et al. Effects of PGC-1alpha on TNF-alpha-induced MCP-1 and VCAM-1 expression and NF-kappaB activation in human aortic smooth muscle and endothelial cells. *Antioxid Redox Signal*. 2007;9:301-307. doi:10.1089/ars.2006.1456
51. Ren FF, Zhao L, Jiang XY, et al. Sphingosylphosphorylcholine alleviates pressure overload-induced myocardial remodeling in mice via inhibiting CaM-JNK/p38 signaling pathway. *Acta Pharmacol Sin*. 2024;45:312-326. doi:10.1038/s41401-023-01168-6
52. Grazette LP, Rosenzweig A. Role of apoptosis in heart failure. *Heart Fail Clin*. 2005;1:251-261. doi:10.1016/j.hfc.2005.03.007

53. Tay KC, Tan LTH, Chan CK, et al. Formononetin: a review of its anticancer potentials and mechanisms. *Front Pharmacol*. 2019;10:820. doi:10.3389/fphar.2019.00820
54. Porter AG, Jänicke RU. Emerging roles of caspase-3 in apoptosis. *Cell Death Differ*. 1999;6:99-104. doi:10.1038/sj.cdd.4400476
55. Ranjbar Bushehri M, Babaei N, Esmaeili Gouvarchin Ghaleh H, Khamisipour G, Farnoosh G. Anti-inflammatory activity of peiminine in acetic acid-induced ulcerative colitis model. *Inflammopharmacology*. 2024;32:657-665. doi:10.1007/s10787-023-01360-4
56. Yang J, Nie J, Ma X, Wei Y, Peng Y, Wei X. Targeting PI3K in cancer: mechanisms and advances in clinical trials. *Mol Cancer*. 2019;18:26. doi:10.1186/s12943-019-0954-x
57. Chen S, Peng J, Sherchan P, et al. TREM2 activation attenuates neuroinflammation and neuronal apoptosis via PI3K/Akt pathway after intracerebral hemorrhage in mice. *J Neuroinflammation*. 2020;17:168. doi:10.1186/s12974-020-01853-x
58. Jiang K, Guo S, Yang C, et al. Barbaloin protects against lipopolysaccharide (LPS)-induced acute lung injury by inhibiting the ROS-mediated PI3K/AKT/NF-κB pathway. *Int Immunopharmacol*. 2018;64:140-150. doi:10.1016/j.intimp.2018.08.023
59. Wang K, Chai L, Qiu Z, Zhang Y, Gao H, Zhang X. Overexpression of TRIM26 suppresses the proliferation, metastasis, and glycolysis in papillary thyroid carcinoma cells. *J Cell Physiol*. 2019;234:19019-19027. doi:10.1002/jcp.28541
60. Venugopal R, Jaiswal AK. Nrf2 and Nrf1 in association with Jun proteins regulate antioxidant response element-mediated expression and coordinated induction of genes encoding detoxifying enzymes. *Oncogene*. 1998;17:3145-3156. doi:10.1038/sj.onc.1202237
61. Vashi R, Patel BM. NRF2 in cardiovascular diseases: a ray of Hope! *J Cardiovasc Transl Res*. 2021;14:573-586. doi:10.1007/s12265-020-10083-8
62. Chang W, Wu QQ, Xiao Y, et al. Acacetin protects against cardiac remodeling after myocardial infarction by mediating MAPK and PI3K/Akt signal pathway. *J Pharmacol Sci*. 2017;135:156-163. doi:10.1016/j.jphs.2017.11.009
63. McLean BA, Kienesberger PC, Wang W, et al. Enhanced recovery from ischemia-reperfusion injury in PI3Kα dominant negative hearts: investigating the role of alternate PI3K isoforms, increased glucose oxidation and MAPK signaling. *J Mol Cell Cardiol*. 2013;54:9-18. doi:10.1016/j.yjmcc.2012.10.015
64. Li Y, Xia J, Jiang N, et al. Corin protects H(2)O(2)-induced apoptosis through PI3K/AKT and NF-κB pathway in cardiomyocytes. *Biomed Pharmacother*. 2018;97:594-599. doi:10.1016/j.biopha.2017.10.090
65. Brigelius-Flohé R, Flohé L. Basic principles and emerging concepts in the redox control of transcription factors. *Antioxid Redox Signal*. 2011;15:2335-2381. doi:10.1089/ars.2010.3534
66. Bellezza I, Mierla AL, Minelli A. Nrf2 and NF-κB and their concerted modulation in cancer pathogenesis and progression. *Cancers (Basel)*. 2010;2:483-497. doi:10.3390/cancers2020483
67. Zhang Z, Yang Z, Wang S, Wang X, Mao J. Targeting MAPK-ERK/JNK pathway: a potential intervention mechanism of myocardial fibrosis in heart failure. *Biomed Pharmacother*. 2024;173:116413. doi:10.1016/j.biopha.2024.116413

SUPPORTING INFORMATION

Additional supporting information can be found online in the Supporting Information section at the end of this article.

How to cite this article: Wang Y, Feng X, Zhao S, et al. Chrysin alleviates pressure overload–induced myocardial remodeling through regulating the PI3K/AKT/NRF2 pathway–mediated oxidative stress response. *Anim Models Exp Med*. 2026;9:1373-1394. doi:10.1002/ame2.70230